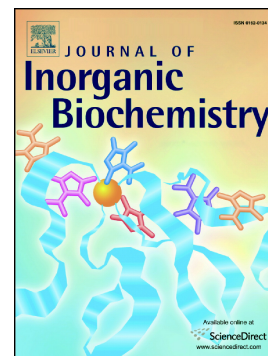


Zn(II) complexes of
(E)-4-(2-(pyridin-2-ylmethylene)hydrazinyl)quinazoline in
combination with non-steroidal anti-inflammatory drug sodium
diclofenac: Structure, DNA binding and photo-cleavage studies,
antioxidant activity and interaction with albumin



Chrisoula Kakoulidou, Panagiotis S. Gritzapis, Antonios G.
Hatzidimitriou, Konstantina C. Fylaktakidou, George Psomas

PII: S0162-0134(20)30222-1

DOI: <https://doi.org/10.1016/j.jinorgbio.2020.111194>

Reference: JIB 111194

To appear in: *Journal of Inorganic Biochemistry*

Received date: 26 May 2020

Revised date: 29 June 2020

Accepted date: 13 July 2020

Please cite this article as: C. Kakoulidou, P.S. Gritzapis, A.G. Hatzidimitriou, et al., Zn(II) complexes of (E)-4-(2-(pyridin-2-ylmethylene)hydrazinyl)quinazoline in combination with non-steroidal anti-inflammatory drug sodium diclofenac: Structure, DNA binding and photo-cleavage studies, antioxidant activity and interaction with albumin, *Journal of Inorganic Biochemistry* (2020), <https://doi.org/10.1016/j.jinorgbio.2020.111194>

This is a PDF file of an article that has undergone enhancements after acceptance, such as the addition of a cover page and metadata, and formatting for readability, but it is not yet the definitive version of record. This version will undergo additional copyediting, typesetting and review before it is published in its final form, but we are providing this version to give early visibility of the article. Please note that, during the production process, errors may be discovered which could affect the content, and all legal disclaimers that apply to the journal pertain.

Zn(II) complexes of (*E*)-4-(2-(pyridin-2-ylmethylene)hydrazinyl)quinazoline in combination with non-steroidal anti-inflammatory drug sodium diclofenac: Structure, DNA binding and photo-cleavage studies, antioxidant activity and interaction with albumin

Chrisoula Kakoulidou,^a Panagiotis S. Gritzapis,^b Antonios G. Hatzidimitriou,^a Konstantina C. Fylaktakidou,^{b,c,*} George Psomas,^{a,*}

^a *Laboratory of Inorganic Chemistry, Faculty of Chemistry, Aristotle University of Thessaloniki, GR-54124 Thessaloniki, Greece.*

^b *Laboratory of Organic, Bioorganic and Natural Product Chemistry, Molecular Biology and Genetics Department, Democritus University of Thrace, University Campus, Dragana, GR-68100 Alexandroupolis, Greece.*

^c *Laboratory of Organic Chemistry, Faculty of Chemistry, Aristotle University of Thessaloniki, GR-54124 Thessaloniki, Greece*

Abstract

The interaction of the novel quinazoline (*E*)-4-(2-(pyridin-2-ylmethylene)hydrazinyl)quinazoline (**L**) with Zn²⁺ was performed in the absence or presence of the non-steroidal anti-inflammatory drug sodium diclofenac (Nadicl) and resulted in the formation of the complexes [Zn(L)₂](NO₃)₂·MeOH (**1**·MeOH) and [Zn(L)(dicl-O)₂]·MeOH (**2**·MeOH), respectively. The two complexes were characterized by IR and ¹H NMR spectroscopy and by single-crystal X-ray crystallography. In these complexes, **L** was tridentately coordinated to Zn(II) *via* the quinazoline, hydrazone and pyridine nitrogen atoms. Further studies concerning the behavior of the compounds towards calf-thymus (CT) DNA and supercoiled circular pBluescript KS II plasmid DNA (pDNA) have been performed. The complexes may bind to CT DNA *via* intercalation, with complex **1** showing higher binding affinity than **2**. The complexes may cleave pDNA in the absence or presence of irradiation with UVA, UVB or visible light and the most active pDNA-cleavager is compound **1**. The binding constants of the compounds for bovine serum albumin were calculated and the subdomain of the albumin where the compounds prefer to bind was determined. The free radical scavenging ability of the compounds was evaluated towards 1,1-diphenyl-picrylhydrazyl and 2,2'-azinobis-(3-ethylbenzothiazoline-6-sulfonic acid) radicals with

* Corresponding authors' e-mails:

kfylakta@chem.auth.gr (K.C. Fylaktakidou); gepsomas@chem.auth.gr (G. Psomas)

complex **2** being the most active compound. Thus, complex of type **1** maybe a lead compound for the development of novel DNA-binders and DNA-cleavers or photo-cleavers for medical and biotechnological “on demand” applications, whereas the structure of complex type **2** may provide novel antioxidants and radical scavengers.

Keywords: Quinazoline derivatives; Zn(II) complexes; interaction with calf-thymus DNA; plasmid DNA-photocleavage; interaction with albumin; free radical scavenging

1 Introduction

Quinazoline is an *N*-heterocyclic compound that contains two fused aromatic rings of benzene and pyrimidine [1] and was first prepared in 1869 by Griess [2]. It was in 1903 when Gabriel and Colman developed a more satisfactory synthetic route of quinazoline [3]. Since then, new quinazoline derivatives were reported, but it has been only a few decades since their use increased because of their biological properties [4]. FDA has approved many quinazoline derivatives as anticancer drugs (i.e. 4-anilinoquinazolines) that their main role is to inhibit activity of EGFR (Epidermal Growth Factor Receptor) as they interact with the ATP-binding site [1].

Hydrazones are known for more than a century and appear in thousands of publications as key structures providing numerous applications owing to their $R^1R^2C=N-NR^3R^4$ functional group. The imine group of hydrazones may allow configurational isomerism which provides molecular switches. Additionally, imine bears both a nucleophilic site for cationic sensing and coordination to metals and an electrophilic site for anionic sensing and finally, an acidic hydrogen ($R^3 = H$) for acid/base sensors or pH switches [5]. Hydrazones are used as linkers in polymeric [6] or in pH responsive drug delivery systems [7], they exhibit voltammetric properties under reductive and oxidative conditions in both aqueous and non-aqueous media [8], whereas their metal complexes have biological, analytical and catalytic applications [9]. The biological activities of hydrazone derivatives have also been extensively reviewed [10-12].

4-Quinazoline-hydrazone hybrid molecules exhibited antiproliferative activity [13], or potent oral activity as inhibitors of phosphodiesterase-4 [14], whereas metal complexation with various metals [15] and Zn [16,17] indicated photoluminescence properties.

Zinc belongs to the essential trace elements according to WHO Classification and Friedan's Classification of Elements and is the second, after iron, most plentiful in humans encountered in numerous zinc proteins in which zinc plays either a catalytic or a structural role [18]. Among the most well-known Zn enzymes are Cu/Zn superoxide dismutase, carbonic anhydrase, and carboxypeptidase [19]. Zn is also bound to metallothioneins, which play an important role in Zn uptake, distribution, storage, and release in cells [20]. Zinc possesses structural role in finger

proteins which are very important because zinc fingers form parts of some transcription factors, which are proteins that recognize DNA-base sequences during DNA-replication and DNA-transcription [21]. Zinc deficiency is associated with many diseases (growth retardation, delayed sexual maturation, infection susceptibility, and diarrhea) [22].

The use of metal complexes as treatment for the therapy of cancer started after the discovery of antiproliferative activity of *cisplatin* [23] followed by analogous Pt complexes as *carboplatin* and *oxaliplatin*. Since then more and more new transition metal complexes have been developed as potential metallodrugs for therapeutic and diagnostic applications for cancer, diabetes, inflammation, cardiovascular, and neurodegenerative diseases [24,25]. As far as Zn incorporated drugs concerns, they are used in the treatment of skin infections and injuries and other infections responsible for children mortality in Asian and African countries with “Baby Zinc” [26]. Furthermore, zinc complexes are reported for the *in vitro* evaluation of potential biological applications including promising antidiabetic [27], anti-inflammatory [28], antimicrobial [29], antioxidant [30] and antiproliferative [31] properties.

DNA is the key target molecule for the development of anticancer, antibacterial and antiviral agents [32]. Depending on the mechanism of action they are divided in inhibitors of nucleotide synthesis (e.g. methotrexate), polymerase inhibitors (e.g. cytarabine), DNA-template damaging agents (e.g. cisplatin) and topoisomerase inhibitors (e.g. doxorubicin) [33]. Within this context, the interaction of small molecules with DNA is usually studied as a preliminary step of possible therapeutic applications [33]. Thus, the structure and the stability of metal complexes are usually crucial in regard to the DNA-interaction mode. Labile ligands may be displaced by DNA-bases leading to covalent DNA-binding (as in the case of cisplatin) [34,35]. When weaker interactions can be developed between the intact complex and DNA, noncovalent interactions with DNA occur, including intercalation (due to π - π stacking interactions between the planar aromatic ring(s) of the compound and the DNA-nucleobases), groove-binding (because of hydrogen bonds or hydrophobic bonds or van der Waals forces) or electrostatic interactions (in the case of Coulomb forces) [34,35]. In addition, DNA-cleavage may also result from the interaction of complexes and DNA. Since DNA is a possible target of photodynamic therapy, the changes of DNA upon interaction followed by irradiation may also provide valuable conclusions [36].

We have targeted, synthesized and characterized a novel *o*-pyridine-hydrazone derivative of 4-quinazoline ligand (**L**), namely (*E*)-4-(2-(pyridin-2-ylmethylene)hydrazinyl)quinazoline (Fig. 1(A)). **L** was carefully designed in order to fulfill certain characteristics, such as novelty, rigidity for possible intercalation with DNA and location of electron donors in proper positions ready to incorporate a metal upon complexation. The metal of choice to examine the chemical reactivity of the ligand was Zn. Noteworthy, a possible complexation is expected a) to shift absorption maxima

at higher wavelengths comparing to the ligand [17] and b) to enhance rigidity and affinity to DNA. These characteristics may hopefully allow us to study a) a possible artificial nuclease activity [37] and/or b) DNA photo-cleavage in medical applicable UVA-vis irradiation [38].

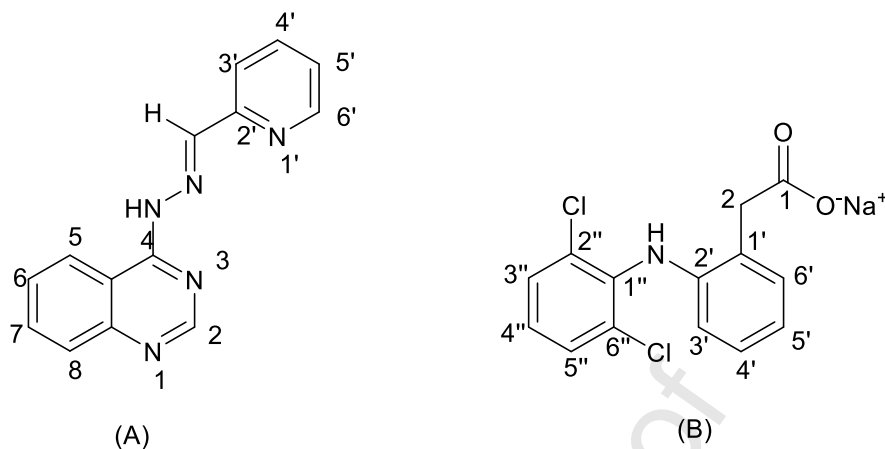


Fig. 1. The syntax formula of (A) the quinazoline derivative (*E*)-4-(2-(pyridin-2-ylmethylene)hydrazinyl)quinazoline (**L**) and (B) sodium diclofenac (Nadicl).

A combination of **L** and Zn with another ligand such as the widespread commercially available non-steroidal anti-inflammatory drug (NSAID) sodium diclofenac (Nadicl) (Fig. 1(B)) has also been designed. Nadicl is used as analgesic, antipyretic and anti-inflammatory agent [39]. In addition, Nadicl is proposed for the treatment of rheumatoid arthritis and osteoarthritis [40,41]. There are a lot of reports concerning the coordination of diclofenac ligand with diverse metal ions, such as copper(II) [42,43], manganese(II/III) [44,45], cadmium(II) [46], tin(IV) [47] and nickel(II) [48]; in most cases, the resultant complexes have shown increased free radical scavenging in comparison to free NSAID. Thus, hybrid quinazoline-hydrazone in combination with Nadicl is expected to provide knowledge towards the reactivity of both ligands while present in the same medium. A successful synergistic complexation would allow the study of a novel complex of two pharmacophores in conjunction with a metal which may hopefully provide novel biological activities and applications.

Accordingly, we have synthesized two coordination compounds of **L** with the biological trace element Zn. Initially, the interaction of **L** with $\text{Zn}(\text{NO}_3)_2$ resulted in the formation of the mononuclear dicationic complex $[\text{Zn}(\text{L})_2](\text{NO}_3)_2 \cdot \text{MeOH}$ (**1**·MeOH). As a next step, and in order to combine the biological potency of Zn-L compound with a bioactive co-ligand, we synthesized the neutral mononuclear mixed-ligand complex $[\text{Zn}(\text{L})(\text{dicl-O})_2] \cdot \text{MeOH}$ (**2**·MeOH) *via* the reaction of **L** with $\text{Zn}(\text{NO}_3)_2$ in the presence of the NSAID sodium diclofenac. The resultant coordination compounds **1**·MeOH and **2**·MeOH were characterized by diverse spectroscopic (IR, ^1H NMR) techniques and single-crystal X-ray crystallography.

The potential biological activity of the novel compounds (**L** and its complexes **1** and **2**) has been mainly focused on their interaction with DNA in regard to: (a) their binding affinity towards calf-thymus (CT) DNA studied by (i) UV-vis spectroscopy, (ii) viscosity measurements and (iii) fluorescence emission spectroscopy for ethidium bromide (EB)-competitive studies and (b) their ability to induce cleavage to supercoiled circular pBluescript KS II plasmid DNA (pDNA) in the absence or presence of irradiation with UVA, UVB and visible light. For the most active compound regarding the pDNA-cleavage activity, i.e. complex **1**, further experiments were carried out in an attempt to elucidate the pDNA-cleavage mechanism. In addition, the binding of the compounds to bovine serum albumin (BSA) was investigated by fluorescence emission spectroscopy in order to calculate the corresponding binding constant and to determine the location of binding site. Furthermore, the scavenging activity of the compounds towards free radicals 1,1-diphenylpicrylhydrazyl (DPPH) and 2,2'-azinobis-(3-ethylbenzothiazoline-6-sulfonic acid) (ABTS) was also evaluated.

2. Experimental

2.1 Materials–instrumentation-physical measurements

All chemicals and solvents were reagent grade and were used as purchased from commercial sources; i.e. 2-aminobenzonitrile, triethylorthoformate, ammonium acetate, hydrazine hydrate, 2-pyridine-carboxaldehyde, p-toluenesulfonic acid monohydrate, sodium diclofenac, $\text{Zn}(\text{NO}_3)_2 \cdot 4\text{H}_2\text{O}$, ZnCl_2 , ibuprofen, trisodium citrate, NaCl, CT DNA, EB, BSA, DPPH, nordihydroguaiaretic acid (NDGA), butylated hydroxytoluene (BHT) from Sigma-Aldrich Co, warfarin, 6-hydroxy-2,5,7,8-tetramethylchromane-2-carboxylic acid (trolox) and ABTS from J&K, and all solvents from Chemlab.

Melting points were measured on a Kofler hot-stage apparatus or a melting point meter M5000 KRÜSS, and are uncorrected. NMR spectra were recorded on an Agilent 500/54 (500 MHz and 125 MHz for ^1H and ^{13}C , respectively) spectrometer using CDCl_3 , and/or DMSO-d_6 as solvent. Chemical shifts are given in ppm and J values in Hz using solvent as an internal reference. High-resolution mass spectra (HRMS) were recorded on micrOTOF GC-MS QP 5050 Shimadzu single-quadrupole mass spectrometer. All reactions were monitored on commercial available pre-coated TLC plates (layer thickness 0.25 mm) of Kieselgel 60 F_{254} . Yields were calculated after recrystallization.

Infrared (IR) spectra ($400\text{--}4000\text{ cm}^{-1}$) were recorded on a Nicolet FT-IR 6700 spectrometer with samples prepared as KBr pellets. UV-visible (UV-vis) spectra were recorded in solution at concentrations in the range 5 mM – 20 μM on a Hitachi U-2001 dual beam spectrophotometer. C, H and N elemental analyses were carried out on a Perkin Elmer 240 B elemental analyzer. Molar

conductivity measurements were carried out in 1 mM DMSO solution of the complexes with a Crison Basic 30 conductometer. Fluorescence spectra were recorded in solution on a Hitachi F-7000 fluorescence spectrophotometer. Viscosity experiments were carried out using an ALPHA L Fungilab rotational viscometer equipped with an 18-mL LCP spindle and the measurements were performed at 100 rpm.

During the photo-cleavage studies, all samples were irradiated with Philips 2×9W/01/2P UV-B narrowband lamps at 312 nm, or BL PL-S 9W/10/2P lamps (2×9 W, Philips, Pila, Poland) at 365 nm, or commercial white light lamps for visible, 15 cm distance.

CT DNA stock solution was prepared by dilution of CT DNA to buffer (containing 150 mM NaCl and 15 mM trisodium citrate at PH 7.0) followed by exhaustive stirring at 4 °C for three days, and kept at 4°C for no longer than eight days. The stock solution of CT DNA gave a ratio of UV absorbance at 260 and 280 nm (A_{260}/A_{280}) equal to 1.88, indicating that the DNA was sufficiently free of protein contamination [49]. The concentration of CT DNA was determined by the UV absorbance at 260 nm after 1:20 dilution using $\epsilon = 6600 \text{ M}^{-1}\text{cm}^{-1}$ [50].

2.2 Synthesis of ligand L

The synthesis of L was accomplished in three steps including also the synthesis of the 4-aminoquinazoline (I) and quinazolin-4-yl-hydrazine (II) as intermediates.

2.2.1 Synthesis of 4-aminoquinazoline, I (1st step)

4-Aminoquinazoline (I) was prepared following the procedure published earlier [51]. More specifically, 2-aminobenzonitrile (6 g, 50.8 mmol) was dissolved in 30 mL ethanol and ammonium acetate (7.83 g, 102 mmol) and triethylorthoformate (15.1g, 102 mmol) were added. The reaction mixture was refluxed at 90 °C for 3.5 h and the solution turned from light yellow to light grey with precipitation of a grey solid. The reaction was monitored by TLC. The mixture was left to cool at room temperature. The solid product was separated by filtration, washed three times with water and ethanol, respectively, and dried *in vacuo* to afford 5.9 g (yield = 78 %) of a light grey solid (I). IR (KBr), ν (cm^{-1}): $\nu(\text{N-H})_{\text{primary}}$: 3373 (medium (m)), 3277 (m); $\delta(\text{N-H})_{\text{primary}}$: 1614 (m); $\nu(\text{C=N})$, 1582 (very strong (vs)); $w(\text{N-H})$: 760 (strong (s)). ¹H NMR (500 MHz), DMSO-*d*₆, δ (ppm): 8.38 (s, 1H, H-2), 8.21 (d, $J = 8.1$ Hz, 1H), 7.76 (t, $J = 7.5$ Hz, 1H), 7.76 (obscured, 2H, NH₂), 7.66 (d, $J = 8.2$ Hz, 1H), 7.48 (t, $J = 7.6$ Hz, 1H).

2.2.2 Synthesis of quinazolin-4-yl-hydrazine, II (2nd step).

Quinazolin-4-yl-hydrazine (II) was prepared following the procedure published elsewhere [52]. 4-Aminoquinazoline I (2 g, 14 mmol) was dissolved in 10 mL of ethanol and an excess of

hydrazine monohydrate was added. The reaction mixture was refluxed in 100 °C for 24 h. The reaction was monitored by TLC. The reaction mixture was slowly allowed to cool to ambient temperature. Yellow crystalline product was precipitated, separated by filtration, washed with cold ethanol/water and dried *in vacuo*. Yield (53%, 1.178 g). IR (KBr), ν (cm⁻¹): $\nu(\text{N-H})_{\text{secondary}}$: 3500 (broad (br)); $\nu(\text{N-H})_{\text{primary}}$: 3320 (m), 3200 (m); $\nu(\text{C-N})$, 1637 (m); $\delta(\text{N-H})_{\text{primary}}$: 1616 (m); $w(\text{N-H})$: 763 (m). ¹H NMR (500 MHz, DMSO-*d*₆), δ (ppm): 9.62 (brs, 1H), 8.47 (brs, 1H), 8.16 (brs, 1H), 7.71 (brs, 1H), 7.65 (brs, 1H), 7.45 (brs, 1H), 4.74 (brs, 2H).

2.2.3 Synthesis of (E)-4-(2-(pyridin-2-ylmethylene)hydrazinyl)quinazoline, **L** (3rd step).

In an ethanolic solution of quinazolin-4-yl-hydrazine (**II**) (350 mg, 2.17 mmol), 2-pyridinecarboxaldehyde (206 μL , 2.17 mmol) was added slowly at 90 °C with continuous stirring in the presence of a few drops of *p*-toluenesulfonic acid as catalyst for 3 h. The reaction was monitored by TLC. The reaction mixture was slowly allowed to cool to ambient temperature. Yellow crystalline product of **L** was separated by filtration, washed with cold ethanol. Drying *in vacuo* afforded 320 mg (yield 61 %) of a yellow solid of **L** which was used without further purification. The compound **L** is soluble in MeOH and DMSO. ¹H NMR (500 MHz, DMSO-*d*₆), δ (ppm): 11.83 (s, 1H, NH), 8.64 (dd, $J = 4.8, 0.7$ Hz, 1H, H-6'), 8.45 (s, 1H, H-2), 8.44 (d, $J = 8.0$ Hz, 1H, H-3'), 8.26 (d, $J = 7.8$ Hz, 1H, H-5), 7.92 (s, 1H, C(**H**)=N), 7.90 (dt, $J = 7.7, 1.2$ Hz, 1H, H-4'), 7.70 (t, $J = 7.2$ Hz, 1H, H-7), 7.54 (d, $J = 8.1$ Hz, 1H, H-8), 7.46 (t, $J = 7.7$ Hz, 1H, H-6), 7.43 (dt, $J = 6.3, 1.1$ Hz, 1H, H-5'). HRMS (ESI) (m/z): calc. for C₁₄H₁₁N₅ [M+H]⁺ 250.1087; found 250.1087. IR (KBr), $\nu(\text{cm}^{-1})$: $\nu(\text{N-H})_{\text{secondary}}$: 3164(m); $\nu(\text{C=N})$: 1623(vs), 1606 (s); $w(\text{N-H})$: 769 (m). UV-vis in DMSO, λ (nm) (ϵ , M⁻¹cm⁻¹): 433 (shoulder (sh)) (1000), 365 (7350), 294 (4500).

2.3 Synthesis of the complexes

2.3.1 Synthesis of [Zn(L)₂](NO₃)₂·MeOH, **1**·MeOH

The complex was synthesized *via* the addition of a methanolic solution (3 mL) of **L** (31 mg, 0.12 mmol) to a methanolic solution of Zn(NO₃)₂·4H₂O (16 mg, 0.06 mmol). After stirring for 15 min, 2 mL of H₂O was added and the mixture was left for slow evaporation. Colorless single-crystals of [Zn(L)₂](NO₃)₂·MeOH (**1**·MeOH) suitable for X-ray structure determination were deposited (17 mg, ~40 %) after one month. The complex is soluble in DMSO ($\Lambda_{\text{M}} = 105$ S·cm²·mol⁻¹, 1 mM in DMSO). Anal. calc. for C₂₉H₂₆N₁₂O₇Zn (MW = 719.98) C, 48.37; H, 3.64; N, 23.35; found: C, 48.52; H, 3.45; N, 23.16 %. IR (KBr), $\nu(\text{cm}^{-1})$: $\nu(\text{N-H})$, 3451 (br); $\nu(\text{C-H})$: 2924 (m); $\nu(\text{C=N})$: 1635 (s), 1614 (vs); $\nu_3(\text{NO}_3)$: 1383 (vs); $\nu_2(\text{NO}_3)$, 823 (m); $w(\text{N-H})$: 751(m); $\rho(\text{C-H})_{\text{out-of-plane,py}}$: 691 (m). UV-vis in DMSO, λ (nm) (ϵ , M⁻¹cm⁻¹): 454 (2900), 430 (sh) (2500), 402(sh)

(2700), 371 (3200), 295 (2700). ^1H NMR (500 MHz, DMSO- d_6), δ (ppm): 13.32 (brs, 1H, NH), 9.16 (s, 1H, H-2), 8.40 (d, $J = 8.0$ Hz, 1H, H-5), 8.17-8.11 (m, 3H, C(H)=N, H-4', H-6'), 8.06 (d, $J = 7.5$ Hz, 1H, H-3'), 7.86 (t, $J = 7.5$ Hz, 1H, H-7), 7.65 (t, $J = 6.8$ Hz, 1H, H-6), 7.55-7.53 (m, 2H, H-5', H-8).

2.3.2 Synthesis of $[\text{Zn}(\text{L})(\text{dicl})_2]\cdot\text{MeOH}$, $2\cdot\text{MeOH}$

In a methanolic solution (5 mL) of ZnCl_2 (22 mg, 0.16 mmol), the methanolic solutions (7 mL) of sodium diclofenac (100 mg, 0.32 mmol) and **L** (40 mg, 0.16 mmol) were added simultaneously. The yellow solution was left to evaporate slowly in ambient temperature. Colorless single-crystals of $2\cdot\text{MeOH}$ (80 mg, ~55 %) suitable for X-ray crystallography were collected after 40 days. The complex is soluble in DMSO ($\Lambda_{\text{M}} = 10 \text{ S}\cdot\text{cm}^2\cdot\text{mol}^{-1}$, 1 mM in DMSO). Anal. calc. for $\text{C}_{43}\text{H}_{35}\text{Cl}_4\text{N}_7\text{O}_5\text{Zn}$ (MW = 936.99) C, 55.12; H, 3.77; N, 10.47; found: C, 55.45; H, 3.85; N, 10.64 %. IR (KBr), $\nu(\text{cm}^{-1})$: $\nu(\text{N-H})$: 3284 (m); $\nu(\text{C=N})$: 1635 (m), 1609 (s); $\nu_{\text{asym}}(\text{CO}_2)_{\text{dicl}}$: 1577 (s); $\nu_{\text{sym}}(\text{CO}_2)_{\text{dicl}}$: 1376 (m); $\Delta\nu(\text{CO}_2) = \nu_{\text{asym}}(\text{CO}_2) - \nu_{\text{sym}}(\text{CO}_2) = 201$; $w(\text{N-H})$: 744(m). UV-vis in DMSO, $\lambda(\text{nm})$ (ϵ , $\text{M}^{-1}\text{cm}^{-1}$): 454 (4050), 432 (sh) (3400), 289 (4400).

2.4 X-ray crystal structure determination

Crystals of **1** and **2** with suitable dimensions was carefully selected and glued to a thin glass fiber. Reflection intensity data were collected on a Bruker Kappa APEX II area-detector diffractometer with a Mo fine focus source ($\lambda = 0.71073 \text{ \AA}$) at ambient temperature [53]. Reflections were collected by using the ω and ϕ scan modes. The structure was solved by direct methods using the SUPERFLIP program in the Crystals package and refined by full-matrix least-squares methods based on F^2 with the Crystals v14.61 build 6236 crystallographic software package [54,55]. All non-hydrogen fully occupied atoms were refined anisotropically. Hydrogen atoms of solvent molecules were found at reasonable positions in the differential Fourier map and located there. Other hydrogen atoms were positioned geometrically and refined using a riding model. All the hydrogen atoms were assigned with isotropic displacement factors due to their pivot atoms and included in the final refinement. Crystallographic and experimental details are summarized in Table S1.

2.5 CT DNA-binding studies

A range of techniques (UV-vis spectroscopy, viscosity measurements and EB-competitive studies) were used in order to investigate the interaction of compounds with DNA and figure out possible bindings modes.

UV-vis spectra of CT DNA (0.15-0.18 mM) were recorded after the addition of each compound in increasing [complex]/[DNA] ratios ($= r$). The DNA-binding constants (K_b , in M^{-1}) were determined through UV-vis titration by the Wolfe-Shimer equation (eq. S1) [56] and the plots $[DNA]/(\epsilon_A - \epsilon_f)$ versus $[DNA]$ using the UV-vis spectra of the compounds (10-50 μM) recorded in the presence of DNA for diverse $1/r$ values. Control experiments of compounds with DMSO were yielded no changes in CT DNA spectra.

Viscosity measurements of DNA ($[DNA] = 0.1$ mM) in buffer solution (150 mM NaCl and 15 mM trisodium citrate at pH 7.0) were performed monitoring the changes of DNA-viscosity in the absence and in the presence of increasing amounts of the compounds (**L** and its complexes **1** and **2**) up to the value of $r = 0.36$. The recorded data are presented as $(\eta/\eta_0)^{1/3}$ versus r , where η is the viscosity of DNA in the presence of the compound, and η_0 is the viscosity of DNA alone in buffer solution. All measurements were contacted at room temperature.

The competitive studies of compounds **L**, **1** and **2** with EB were investigated by fluorescence emission spectroscopy in order to examine if the complexes may displace EB from its CT DNA-EB conjugate [57]. The CT DNA-EB conjugate was prepared by adding 20 μM EB and 26 μM CT DNA in buffer (150 mM NaCl and 15 mM trisodium citrate at pH 7.0). The intercalating effect of the complexes was studied by adding stepwise a certain amount of a solution of the compound into a solution of the DNA-EB conjugate. The influence of the addition of each compound to the DNA-EB complex solution was obtained by monitoring the changes of the fluorescence emission spectra recorded with excitation wavelength (λ_{ex}) at 540 nm. Compound **L** and its complexes **1** and **2** do not show any fluorescence emission bands at room temperature in solution or in the presence of CT DNA or EB under the same experimental conditions ($\lambda_{ex} = 540$ nm); therefore, the observed quenching is attributed to the displacement of EB from its EB-DNA conjugate. The Stern-Volmer constants (K_{SV} , in M^{-1}) have been calculated according to the linear Stern-Volmer equation (eq. S2) [57] and the plots I_0/I versus $[Q]$. The quenching constants (k_q , in $M^{-1}s^{-1}$) of the complexes were calculated according to eq. S3, since the fluorescence lifetime of the EB-DNA system is $\tau_0 = 23$ ns [58].

2.6. Plasmid DNA-cleavage experiments

2.6.1. Cleavage of supercoiled circular pBluescript KS II DNA by metal complexes

The reaction mixtures (20 μL) containing supercoiled circular pBluescript KS II DNA stock solution (Form I, 50 μM /base pair, ~ 500 ng), compounds, and Tris buffer (25 μM , pH 6.8) in Pyrex vials were incubated for 30 min at 37 $^{\circ}C$, centrifuged, and then irradiated with UVB light (312 nm - 18 W for 30 min) or UVA light (365 nm - 18 W for 2 h) or white light (18 W for 2 h) being at 15 cm distance under aerobic conditions at room temperature.

After addition of the gel-loading buffer [6X Orange DNA Loading Dye 10 mM Tris-HCl (pH 7.6), 0.15% orange G, 0.03% xylene cyanol FF, 60% glycerol, and 60 mM EDTA, by Fermentas], the reaction mixtures were loaded on a 1% agarose gel with EB staining. The electrophoresis tank was attached to a power supply at a constant current (65 V for 1 h). The gel was visualized by 312 nm UV transilluminator and photographed by an FB-PBC-34 camera vilberlourmat. Quantification of DNA-cleaving activities was performed by integration of the optical density as a function of the band area using the program “Image J” available at the site <http://rsb.info.nih.gov/ij/download.html>.

The ss% and ds% damages were calculated according to the following equations (eq. 1) and (eq. 2):

$$ss\% = \frac{FormII}{(FormI+FormII+FormIII)} \times 100 \quad (\text{eq. 1})$$

$$ds\% = \frac{FormIII}{(FormI+FormII+FormIII)} \times 100 \quad (\text{eq. 2})$$

where, as Form II we consider Form II of each series minus Form II of the irradiated control DNA and as Form I, we consider Form I of each series. The amount of supercoiled DNA was multiplied by factor of 1.43 to account for reduced EB intercalation into supercoiled DNA [59].

2.7 Antioxidant biological assay

The antioxidant activity of the compounds was evaluated *via* their ability to scavenge *in vitro* free radicals such as DPPH and ABTS. All the experiments were carried out at least in triplicate and the standard deviation of absorbance was less than 10% of the mean.

2.7.1 Determination of the reducing activity of the stable radical DPPH

To an ethanolic solution of DPPH (0.1 mM) an equal volume solution of the compounds (0.1 mM) in ethanol was added. Absolute ethanol was also used as control solution. The absorbance at 517 nm was recorded at room temperature after 20 and 60 min, in order to examine the possible existence of a potential time-dependence of the DPPH radical scavenging activity [60]. The DPPH scavenging activity of the complexes was expressed as the percentage reduction of the absorbance values of the initial DPPH solution (DPPH%). NDGA and BHT were used as reference compounds.

2.7.2 Assay of radical cation ABTS-scavenging activity

Initially, a water solution of ABTS was prepared (2 mM). ABTS radical cation (ABTS^{•+}) was produced by the reaction of ABTS stock solution with potassium persulfate (0.17 mM) and the mixture was stored in the dark at room temperature for 12-16 h before its use. The ABTS was oxidized incompletely because the stoichiometric reaction ratio of ABTS and potassium persulfate

is 1:0.5. The absorbance became maximal and stable only after more than 6 h of reaction although the oxidation of the ABTS started immediately. The radical was stable in this form for more than 2 days when allowed to stand in the dark at room temperature. Afterwards, the ABTS^{•+} solution was diluted in ethanol to an absorbance of 0.70 at 734 nm and 10 μ L of diluted compounds or standards (0.1 mM) in DMSO were added. The absorbance was recorded out exactly 1 min after initial mixing [60]. The radical scavenging activity of the complexes was expressed as the percentage inhibition of the absorbance of the initial ABTS solution (ABTS%). Trolox was used as an appropriate standard.

2.8 Albumin assays

2.8.1 BSA-binding studies

The albumin-binding study was performed by tryptophan fluorescence quenching experiments using BSA (3 μ M) in buffer (containing 15 mM trisodium citrate and 150 mM NaCl at pH 7.0). The fluorescence emission spectra were recorded with an excitation wavelength of 295 nm. The quenching of the emission intensity of tryptophan residues of BSA at 343 nm was monitored using L or its complexes as quenchers with gradually increasing concentration [57]. Except to this, the fluorescence emission spectra of the compounds were also recorded with $\lambda_{\text{ex}} = 295$ nm and no appreciable emission was observed. The influence of the inner-filter effect on the measurements was evaluated by eq. S4 [61]. The Stern-Volmer and Scatchard equations (eq. S2, S3 and S5) [62] and graphs were used in order to calculate the Stern-Volmer constant K_{SV} (in M^{-1}), the quenching constant k_q (in $\text{M}^{-1}\text{s}^{-1}$), the BSA-binding constant (K , in M^{-1}) and the number of binding sites per albumin n .

2.8.2 Competitive BSA-fluorescence studies with warfarin and ibuprofen

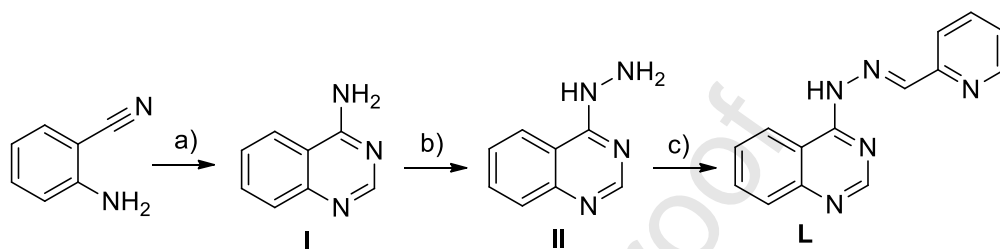
The competitive studies with warfarin or ibuprofen (site probes) were performed by tryptophan fluorescence quenching experiments using a fixed concentration of BSA and site probes (3 μ M) in buffer (containing 15 mM trisodium citrate and 150 mM NaCl at pH 7.0). The fluorescence emission spectra were recorded in the presence of increasing amounts of L or its complexes as quenchers and in the range 300 to 500 nm with an excitation wavelength of 295 nm. The Scatchard equation (eq. S5) [62] and plots were applied on the corrected BSA-fluorescence emission spectra in order to determine the BSA-binding constant (K , in M^{-1}) of the compounds in the presence of warfarin or ibuprofen.

3. Results and discussion

3.1 Synthetic considerations

3.1.1 Synthesis of ligand L

The synthesis of compound **L** was performed in three steps. Initially, the formation of 4-aminoquinazoline **I** was accomplished upon the reaction of commercially available 2-aminobenzonitrile with ammonium acetate in the presence of triethylorthoformate, (78 % yield, Scheme 1) [51,63]. The product without any purification was reacted with hydrazine hydrate to give the corresponding quinazolin-4-yl-hydrazine (**II**) which was then transformed to novel hydrazone **L** upon the reaction with pyridine-2-carboxaldehyde. Compounds **I** and **II** were characterized by NMR and IR spectroscopy. Data obtained for the known compounds were in full accordance with the literature [51,52], while compound **L** was fully characterized.



Scheme 1. Synthesis of compound **L**. a) NH_4OAc , $\text{HC}(\text{OEt})_3$, EtOH reflux, 3.5 h, 78% yield; b) NH_2NH_2 , reflux, 24 h, 53% yield; c) *o*-pyridine carboxaldehyde, *p*-TsOH, EtOH reflux, 3 h, 61 % yield.

3.1.2 Synthesis and characterization of the complexes

Complex **1** was prepared *via* the aerobic reaction of **L** with a methanolic solution of the $\text{Zn}(\text{NO}_3)_2 \cdot 4\text{H}_2\text{O}$ in a 1:2 Zn:L ratio. Complex **2** was afforded *via* the simultaneous addition of **L** and Nadicl into ZnCl_2 in 1:1:2 Zn:L:Nadicl ratio. The composition of the resultant complexes was investigated and confirmed by elemental analysis, IR and ^1H NMR spectroscopy, molecular conductance measurements and single-crystal X-ray crystallography. The compounds are air-stable, soluble mainly in DMSO and insoluble in most common organic solvents and water.

The molar conductivity values of the complexes in 1 mM DMSO solution ($\Lambda_M = 105 \text{ S} \cdot \text{cm}^2 \cdot \text{mol}^{-1}$ for **1** and $10 \text{ S} \cdot \text{cm}^2 \cdot \text{mol}^{-1}$ for **2**) indicate the electrolytic (1:2) nature of complex **1** (since in the case of an 1:2 electrolyte, the Λ_M value of a 1 mM DMSO solution should be $\sim 110 \text{ S} \cdot \text{cm}^2 \cdot \text{mol}^{-1}$ [64]) and the non-electrolytic nature of complex **2** and may show the integrity of the complexes in solution.

The IR spectra of the compounds are rather complex due to the presence of similar different characteristic groups, such as the aromatic quinazoline and the pyridine rings [65]. The assignment of the most characteristic IR peaks was accomplished *via* comparisons with compounds **I** and **II**. In the IR spectra of the complexes, all characteristic bands of the ligand **L** were determined. In addition, in the IR spectrum of complex **2**, the antisymmetric and the symmetric stretching vibration of the carboxylate group of diclofenac ligand gave a $\Delta\nu(\text{CO}_2)$ ($= \nu_{\text{asym}}(\text{CO}_2) - \nu_{\text{sym}}(\text{CO}_2)$) value of

201 cm^{-1} , which is indicative of a monodentate coordination mode of the carboxylate group, as also found in the X-ray crystal structure of the complex [65,66].

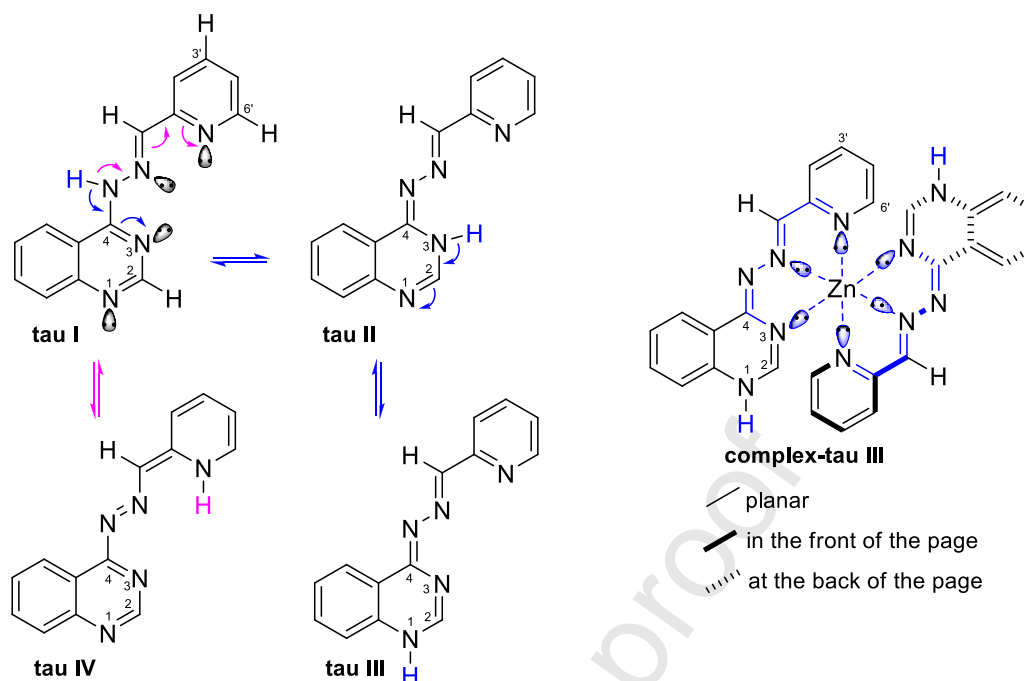


Fig. 2. Tautomeric forms of **L** as free compound (**tau I-IV**) and in complex **1**.

Ligand **L** may exist in four tautomeric forms (**tau I-IV**, Fig. 2). In **tau I**, both quinazoline and pyridine rings retain full aromaticity providing a reason to consider this as a preferred tautomer. The other tautomers result by the migration of the labile H atom found on hydrazone N towards the quinazoline ring nitrogens (N3 and N1, **tau II** and **tau III**, respectively, blue arrows), or towards the pyridine nucleus one (**tau IV**, purple arrows). Careful inspection of **tau III** and **tau IV** allows the recognition, in both of them, of an extended conjugation planar system which may stabilize the whole molecule. Nevertheless, only in **tau III** the three nitrogen lone pairs (pyridine, hydrazone and quinazoline ones) are positioned into the proper planar position which allows eligibility for complexation with Zn.

COSY $^1\text{H-NMR}$ experiments for **L** as well as **1** (Figs. S1 and S2) allowed the assignment of protons were certain differences are observed due to the metal complexation. Thus H-2 proton of quinazoline (8.45 ppm) has shifted downfield in complex **1** (9.16 ppm). The N-H also appears downfielded (11.83 ppm for **L** and 13.32 ppm for **1**) as well as the hydrazone C(H)=N proton (7.93 ppm for **L** and 8.15 ppm for **1**). Complexation of the pyridine nitrogen caused an upfield protection to its neighboring H-6' (8.64 ppm for **L** and ~ 8.13 ppm for **1**). The same phenomenon is observed for H-3' (8.44 ppm for **L** and ~ 8.06 ppm for **1**).

Complex **1** seems to be stable, as we observe no changes in the spectrum when the complex was recorded for diverse time intervals up to 48 h (Fig. S3).

3.2 Crystal structure of the complexes

3.2.1 Crystal structure of 1·MeOH

The molecular structure of compound 1·MeOH, $[\text{Zn}(\text{L})_2](\text{NO}_3)_2 \cdot \text{MeOH}$ was determined by single-crystal X-ray crystallography and is presented in Fig. 3. Selected bond distances and angles are cited in Table 1. The compound crystallizes in the monoclinic system, space group $C2/c$. Compound 1 is constituted by the dicationic complex $[\text{Zn}(\text{L})_2]^{2+}$ which is neutralized by two nitrate ions and contains a solvate methanol molecule.

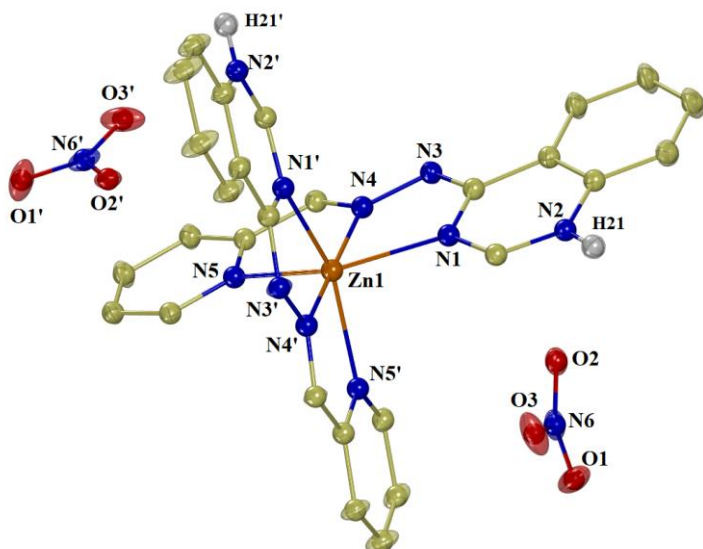


Fig. 3. Molecular structure of compound 1. Hydrogen atoms and solvate molecules are omitted for clarity.

Table 1. Selected bond distances (Å) and angles (°) for complex 1.

Bond	Distance (Å)	Bond	Distance (Å)
Zn1—N5	2.199(2)	N3—N4	1.381(3)
Zn1—N1	2.188(2)	N4—C9	1.278(3)
Zn1—N4	2.070(2)	N3—C8	1.318 (3)
Bond angle	(°)	Bond angle	(°)
N1—Zn1—N1'	95.91(11)	N4—Zn1—N4'	174.30(13)
N1—Zn1—N4	72.57(8)	N4—Zn1—N5	75.73(8)
N1—Zn1—N5	147.97(8)	N4—Zn1—N5'	108.47(8)
N1—Zn1—N4'	103.47(8)	N5—Zn1—N5'	89.97(11)
N1—Zn1—N5'	95.72(8)		

Symmetry code: (') $-x+1, y, -z+3/2$.

In $[\text{Zn}(\text{L})_2]^{2+}$, the Zn(II) atom is six-coordinate with a distorted octahedral geometry. Zn(II) coordination environment consists of two tridentate chelating ligands **L**. Each ligand **L** is

coordinated to Zn through three different nitrogen atoms; the quinazoline N1, the hydrazine N4 and the pyridine N5. On the basis of the Zn-N bond distances, the equatorial plane of the octahedron may be formed by two quinazoline nitrogen atoms N1 and N1', two pyridine nitrogen atoms N5 and N5', while the hydrazine nitrogen N4 and N4' (they are in *trans* positions to each other with an angle of 174.30(13)°) may possess the axial positions offering a slight compression to octahedron (the Zn1—N4 is shorter by ~0.1 Å than the Zn1—N1 and Zn1—N5 distances).

The two nitrate ions are stabilized by hydrogen bonds that are formed between O1 atom of the nitrate anion and H21 of the quinazoline ring N2 or with the hydroxyl H4) of the solvate methanol (Table S2).

3.2.2 Crystal structure of complex 2·MeOH

Complex 2 was crystallized in triclinic system, space group P-1. The structure of complex 2 is presented in Fig. 4 and selected bond distances and angles are summarized in Table 2.

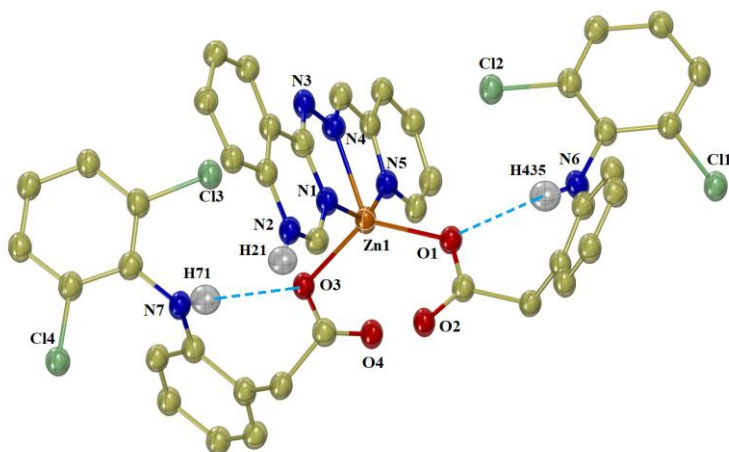


Fig. 4. Molecular structure of complex 2. Hydrogen atoms and solvate molecules are omitted for clarity. The intraligand H-bonds are in dotted light blue lines.

Table 2. Selected bond distances and angles for complex 2.

Bond	Distance (Å)	Bond	Distance (Å)
Zn1—N1	2.169(4)	Zn1—O3	1.997(3)
Zn1—N4	2.133(3)	N3—N4	1.362(5)
Zn1—N5	2.238(4)	N4—C9	1.270(5)
Zn1—O1	1.950(3)		
Bond angle	(°)	Bond angle	(°)
O1—Zn1—O3	121.30(11)	O3—Zn1—N1	91.44(13)
O1—Zn1—N1	102.56(12)	O3—Zn1—N4	117.52(12)
O1—Zn1—N4	121.03(12)	O3—Zn1—N5	103.59(12)
O1—Zn1—N5	94.48(12)	N1—Zn1—N4	71.50(13)

N4—Zn1—N5

75.52(14)

N1—Zn1—N5

147.02(13)

The asymmetric unit of the compound consists of one zinc atom, one neutral tridentate ligand **L** and two deprotonated monodentate diclofenac ligands and a solvate methanol molecule. The zinc atom is five-coordinate and its coordination sphere consists of three nitrogen atoms of the tridentate bis-chelating quinazoline ligand, i.e. the pyridine nitrogen (N5), the hydrazine nitrogen (N4) and the quinazoline nitrogen (N1), and two carboxylate oxygen atoms (O1 and O3) from two monodentate deprotonated diclofenac ligands. Based on the value of the trigonality index [$\tau = (\varphi_1 - \varphi_2)/60^\circ$, φ_1 and φ_2 are the largest angles in the coordination sphere; $\tau = 0$ is found for a perfect square pyramid and $\tau = 1$ for a perfect trigonal bipyramid] [67] $\tau = 0.429$ ($= (147.02^\circ - 121.30^\circ) / 60^\circ$), the geometry around Zn1 may be described as intermediate between square pyramidal and trigonal bipyramidal geometry.

The structure of complex **2** is further stabilized by the existence of diverse (intraligand and intermolecular) hydrogen bonds (Table S2). More specifically, intraligand H-bond are developed in the two diclofenac ligands between the coordinated carboxylate oxygen atoms O1 and O3 and the imino H atoms H435 and H71, respectively. The non-coordinated oxygen atoms O4 and O2 of the two diclofenac ligands participate in intermolecular H-bonds with hydroxyl H434 the MeOH solvate molecule and the quinazoline H21 of the **L** ligand from a neighboring molecule, respectively.

3.4 Interaction of compounds with CT DNA

The binding affinity of complexes with DNA may be the basis for a range of potential biomedical application. Within this context, the affinity of **L** and its complexes **1** and **2** to bind to the CT DNA has been studied *in vitro* by UV-vis spectroscopy, viscosity measurements and *via* their ability to displace the EB when this is conjugated with DNA.

UV-vis spectroscopy is one of the most common techniques to start investigating the interaction, the binding mode and the strength of the compounds with CT DNA through titration and is a convenient method to calculate the DNA-binding constant (K_b). Any changes detected in the DNA-band or the intraligand transition bands of the compounds may declare the existence of interaction as well as its possible binding mode. The UV-vis spectra of CT DNA solutions in the presence of compound **2** at increasing r values are demonstrated representatively in Fig. S4. The CT DNA band is detected at $\lambda_{\max} = 258$ nm in the UV spectra of the CT DNA solution. Upon addition of increasing amounts of **2**, a slight hypochromism is detected accompanied by a red-shift. Similar features are also observed in the UV spectra of a CT DNA solution in the presence of **L** and **1**.

On the hand, the UV spectra of the compounds were recorded in the presence of increasing amounts of a CT DNA solution, i.e. diverse $1/r$ ($= [\text{DNA}]/[\text{compound}]$) values (Fig. S5). In the UV spectra of the compounds in the presence of CT DNA, the interaction of the compounds is evident from the spectral changes observed. The intraligand bands of the complexes exhibit noteworthy hypochromism and/or hyperchromism, which are sometimes accompanied by slight blue- or red-shift (Table 3).

Table 3. UV-vis spectral features of the interaction of **L** and its complexes **1-2** with CT DNA. UV-band (λ in nm) (percentage of the observed hyper-/hypo-chromism ($\Delta A/A_0$, %), blue-/red-shift of the λ_{max} ($\Delta\lambda$, nm)) and DNA-binding constants (K_b).

Compound	Band ($\Delta A/A_0$ ^a , $\Delta\lambda$ ^b)	K_b (M^{-1})
L	294 (-3, -2); 365 (-8, 0); 433(sh ^c) (+5, 0)	$5.70 (\pm 0.27) \times 10^5$
1	295 (-7, -2); 371 (-50, elm ^d); 430(sh) (+80, 0); 454 (+90, 0)	$1.07 (\pm 0.10) \times 10^6$
2	289 (+11, -2); 432 (-13, -1); 454 (-19, -6)	$6.93 (\pm 0.12) \times 10^5$

^a “+” denotes hyperchromism, “-” denotes hypochromism

^b “+” denotes red-shift, “-” denotes blue-shift

^c “sh” = shoulder

^d “elm” = eliminated

The overall changes in the UV-vis spectra of CT DNA may divulge the interaction of the compounds with DNA showing the formation of a compound-DNA conjugate with a subsequent stabilization of DNA double helix. Nevertheless, because of the presence of many transition bands in the spectra of the compounds which show hypochromism or hyperchromism, a discrete fashion of the DNA-binding cannot be safely suggested and more studies concerning the potent complex-DNA interaction are required in order to define the interaction mode. Therefore, DNA-viscosity measurements and competitive studies with EB were performed [68].

The DNA-binding constants (K_b) of compounds (Table 3) have been calculated by the Wolfe-Shimer equation (eq. S1) [64] and the corresponding plots $[\text{DNA}]/(\epsilon_A - \epsilon_f)$ versus $[\text{DNA}]$ (Fig. S6). In brief, the K_b values for the compounds under study are high with the complexes exhibiting higher affinity for CT DNA than free **L**. Further, the K_b constants are higher than that of the classical intercalator EB ($= 1.23 \times 10^5 M^{-1}$) as calculated by Dimitrakopoulou et al [69]. In addition, complex **1** presents the highest K_b among the compounds showing that the existence of diclofenac ligands does not lead to enhanced affinity for CT DNA compared to free **L**. The value of K_b of Zn-diclofenac complex **2** is within the range of metal-diclofenac complexes reported so far [42-44,48].

In order to illustrate the binding mode of the compounds with CT DNA, viscosity measurements of a CT DNA solution were carried out. Viscosity measurements are sensitive to

length variations of CT DNA constituting it as one of the most reliable techniques to investigate the interaction mode between compounds and DNA. Significant increase in DNA-viscosity results from classic intercalation agents that penetrate among DNA-bases increasing the overall DNA-length [42]. Less pronounced or no changes in CT DNA-viscosity are usually due to nonclassical intercalation (i.e. groove-binding or electrostatic interactions) [70].

The viscosity of a CT DNA solution (0.1 mM) was monitored upon addition of increasing amounts of the compounds (up to the value of $r = 0.36$, Fig. 5). The results demonstrate that complexes **1** and **2** provoke notable increase on the relative CT DNA-viscosity with complex **2** inducing the higher increase. On the other hand, the presence of **L** seems to have no significant effect on the relative CT DNA-viscosity. Therefore, we may suggest that complexes **1** and **2** may interact with CT DNA *via* intercalation, whereas **L** probably interacts by nonclassical intercalation [42,70].

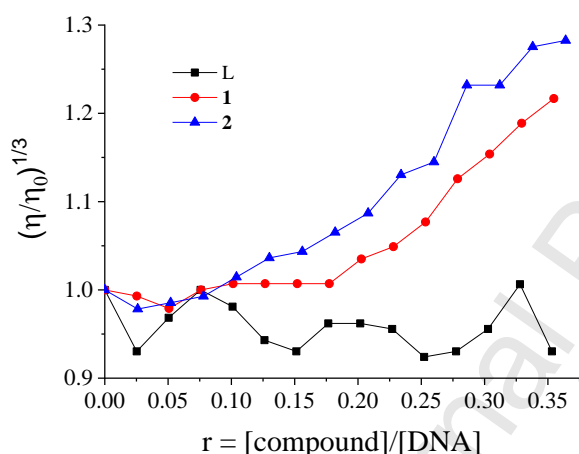


Fig. 5. Relative viscosity $(\eta/\eta_0)^{1/3}$ of CT DNA (0.1 mM) in buffer solution (150 mM NaCl and 15 mM trisodium citrate at pH 7.0) in the presence of the compounds at increasing amounts ($r = [\text{compound}]/[\text{DNA}]$).

A plethora of intercalators has been used as drugs rendering intercalation agents an important type of DNA-binding. Classical intercalators have usually three-to-four fused aromatic rings that can stack with DNA-base pairs at the intercalation site. EB is a conventional classical DNA-intercalator as it binds to two neighboring G-C DNA-base pairs. In order to have a complete interpretation of the binding mode of our compounds, EB-displacement studies were carried out by fluorescence emission spectroscopy [57]. EB exhibits a low fluorescence emission band at ~605 nm when excited at 540 nm while DNA has a weak or no fluorescence despite the fact that look like fluorophores.

The EB-DNA conjugate was formed after pre-treatment of an EB solution ($[\text{EB}] = 20 \mu\text{M}$) with CT DNA ($[\text{DNA}] = 26 \mu\text{M}$) for 1 h and exhibits an intense fluorescence emission band at 592-

595 nm, when excited at 540 nm. The fluorescence emission spectra ($\lambda_{\text{exc}} = 540 \text{ nm}$) of the EB-DNA solution were recorded in the presence of increasing amounts of the compounds (representatively shown for **2** in Fig 6(A)). The addition of the compounds induced moderate (for **L**) and significant (for the complexes) quenching of the fluorescence emission band of the EB-DNA compound with complex **2** showing the most pronounced quenching (Fig. 6(B) and Table 4).

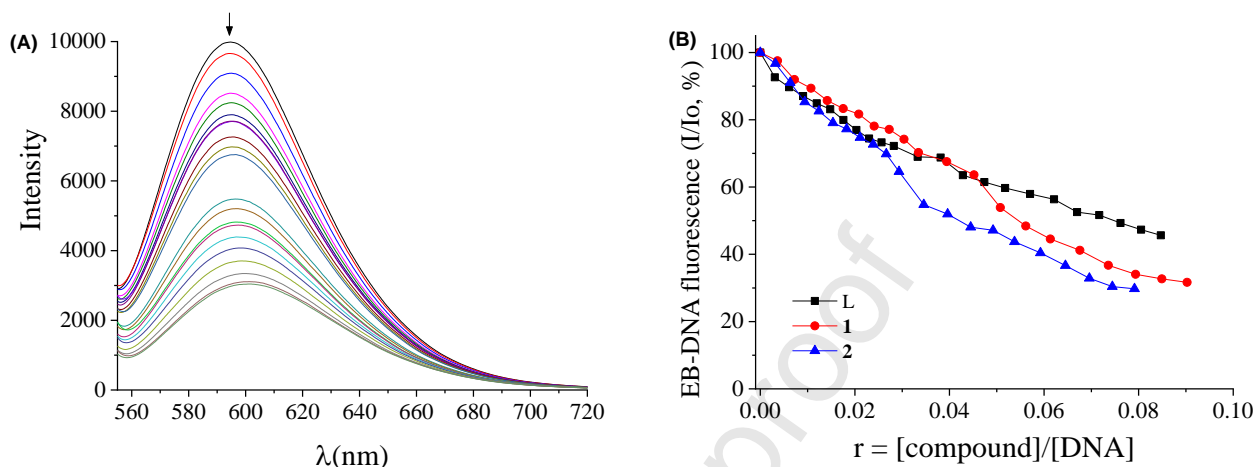


Fig. 6. (A) Fluorescence emission spectra ($\lambda_{\text{exc}} = 540 \text{ nm}$) for EB-DNA ($[\text{EB}] = 20 \mu\text{M}$, $[\text{DNA}] = 26 \mu\text{M}$) in buffer solution in the absence and presence of increasing amounts of complex **2** (up to the value of $r = 0.08$). The arrow shows the changes of intensity upon increasing amounts of **2**. (B) Plot of relative EB-DNA fluorescence intensity (I/I_0 , %) at $\lambda_{\text{em}} = 592 \text{ nm}$ versus r ($r = [\text{compound}]/[\text{DNA}]$) in buffer solution (150 mM NaCl and 15 mM trisodium citrate at pH 7.0) in the presence of **L** and its complexes **1** and **2** (up to 45.6% of the initial EB-DNA fluorescence for **L**, 31.7 % for **1**, and 29.8% for **2**).

Table 4. Percentage of EB-DNA fluorescence quenching ($\Delta I/I_0$, %), Stern-Volmer constants (K_{SV}) and quenching constants of the EB-DNA fluorescence (k_q) for **L** and its complexes **1** and **2**.

Compound	$\Delta I/I_0$ (%)	$K_{\text{sv}} (\text{M}^{-1})$	$k_q (\text{M}^{-1}\text{s}^{-1})$
L	54.4%	$1.05(\pm 0.03) \times 10^5$	$1.05(\pm 0.03) \times 10^{13}$
1	68.3%	$7.60(\pm 0.35) \times 10^4$	$7.60(\pm 0.35) \times 10^{12}$
2	70.2%	$4.23(\pm 0.11) \times 10^5$	$1.84(\pm 0.05) \times 10^{13}$

The observed quenching of the EB-DNA fluorescence emission band is in good agreement with the linear Stern-Volmer equation (eq. S2) [57] as shown in the corresponding Stern-Volmer plots ($R \sim 0.99$, Fig. S7). The EB-DNA quenching constants of the compounds (k_q) have been calculated according to eq. S3, where the fluorescence lifetime of EB-DNA system has the value $\tau_0 = 23 \text{ ns}$ [58]. The k_q constants (Table 4) are significantly higher than $10^{10} \text{ M}^{-1}\text{s}^{-1}$ suggesting, thus, that the quenching of the EB-DNA fluorescence induced from the complexes takes place *via* a static mechanism which leads to the formation of a new conjugate, obviously between DNA and each

complex, verifying indirectly the EB-displacement and subsequently the intercalation of the complexes to CT DNA.

3.5 Interaction of the compounds with plasmid DNA

3.5.1 Plasmid DNA-cleavage activity of the compounds

DMSO solutions of the compounds in different concentrations (500 μ M and 300 μ M) were mixed with a Tris buffer solution (25 μ M, pH= 6.8) containing the supercoiled circular pBLuescript KS II DNA (Form I). Plasmid DNA was analyzed by gel electrophoresis on 1% agarose stained with EB (Fig. 7). All experiments were carried out in triplicate. The supercoiled pDNA in an agarose gel during electrophoresis is shown with Form I. In general, the addition of compounds may result in single-stranded (ss) nicks in the supercoiled DNA leading the formation of the relaxed circular DNA (Form II) and/or double-stranded (ds) nicks forming thus linear DNA (Form III).

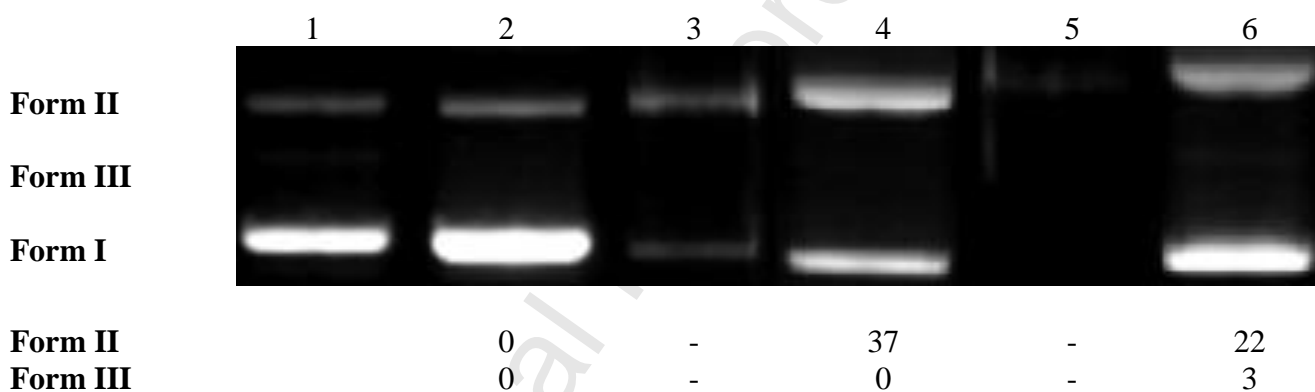


Fig. 7. Agarose gel electrophoretic pattern of EB-stained plasmid DNA (pBLuescript KS II DNA) with **L** and complexes **1-2** at 500 μ M and 300 μ M, after 60 min of electrophoresis. Top: Gel electrophoresis pictures: Lane 1: DNA; Lane 2: DNA + **L** (500 μ M); Lane 3: DNA + complex **1** (500 μ M); Lane 4: DNA + complex **1** (300 μ M); Lane 5: DNA + complex **2** (500 μ M); Lane 6: DNA + complex **2** (300 μ M). Bottom: Calculation of the % conversion to ss and ds damage. DNA forms: Form I = supercoiled, Form II = relaxed, Form III = linear plasmid DNA.

The quinazoline compound **L** did not show any noteworthy effect on pDNA even at 500 μ M (Fig. 7, lane 2). On the other hand, the application of complexes **1** and **2**, especially at the higher concentration used (500 μ M) seems to destroy plasmid DNA in many fragments, thus not allowing EB to be easily detected (Fig. 7, lanes 3 and 5). At the lower concentration applied (300 μ M), complexes **1** and **2** provoke single-stranded nicks 37 % and 22 % for **1** and **2**, respectively (Fig. 7, lanes 4 and 6).

3.5.2 Plasmid DNA photo-cleavage studies

DMSO solutions of the compounds in different concentrations (500 μM and 300 μM) were mixed with a Tris buffer solution (25 μM , pH = 6.8) containing the supercoiled circular pBLuescript KS II DNA (Form I). This mixture was irradiated at room temperature with UVB light (312 nm) for 30 min or UVA light (365 nm) for 2 h or visible light (400-800 nm) for 2 h, under aerobic conditions. Plasmid DNA was analyzed by gel electrophoresis on 1 % agarose stained with EB. All experiments were carried out at least three times. The electrophoresis pictures of control pDNA are given in Fig. S8.

As we have discussed before (3.5.1), the ligand **L** did not show any noteworthy effect on pDNA even at 500 μM , in dark. The same happened upon irradiation with UVB (312 nm) and UVA light (365 nm). Nevertheless, irradiation with visible light resulted in a moderate pDNA-photocleaving activity for **L** ~40% damage (data not shown).

Agarose gel electrophoresis images, for the photo-irradiation of complexes **1** and **2** are shown in Fig. 8. We may observe that, at a concentration of 300 μM , irradiation of complex **1** at 312 nm improved the cleavage ability of the compound comparing to the dark (Fig. 8, **1**-312 nm and **1**-dark, respectively). In a similar way, irradiation at 365 nm was also beneficial for DNA-cleavage. In order to gain the same photo-cleavage result with visible light we had to increase the concentration of complex **1** at 500 μM (Fig. 8, **1**-365 nm and **1**-visible, respectively), in order to overcome the loss of UV absorption.

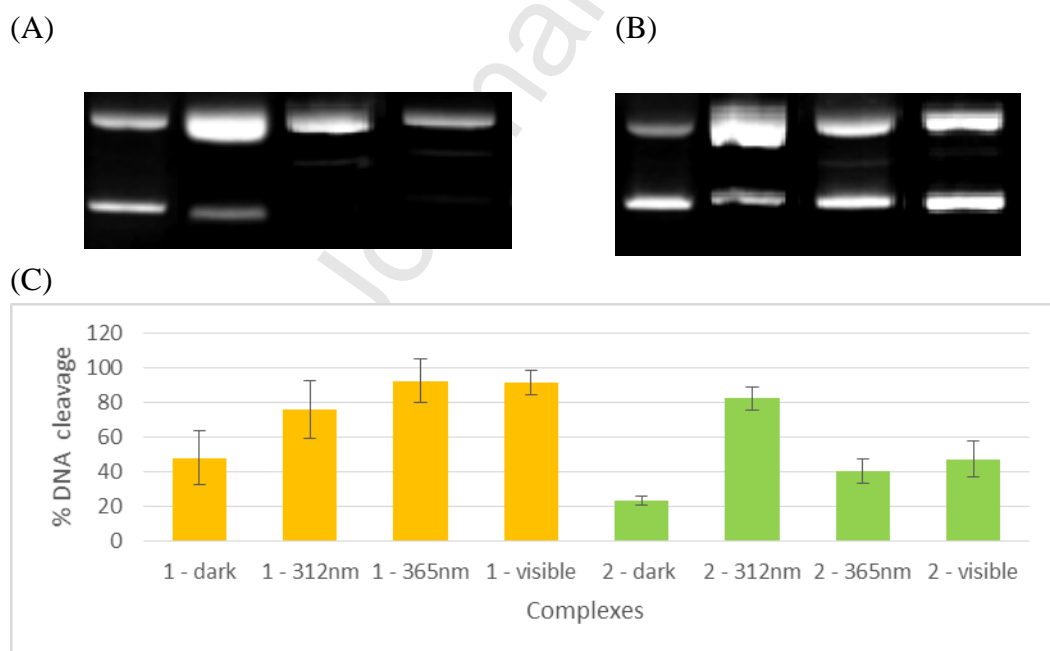


Fig. 8. (A) pDNA (pBLuescript KS II DNA) cleavage and photo-cleavage induced by complex **1** at 300 μM in absence of irradiation and after irradiation with UVB light (312 nm), UVA light (365nm) and visible light respectively. (B) pDNA (pBLuescript KS II DNA) cleavage and photocleavage induced by complex **2** at 300 μM in absence of irradiation and after irradiation with UVB light (312 nm), UVA light (365 nm) and (C) (ss + ds) % DNA cleavage caused by complexes **1** and **2** (300 μM , except complex **2** irradiation with visible light at 500 μM).

As far as complex **2** concerns, compared to dark, it presented a rather high increase of cleavage activity when irradiated at 312 nm (300 μ M), whereas the activity was decreased at 365 nm (300 μ M) and visible light (500 μ M) (Fig. 8, **2-dark**, **2-312 nm**, **2-365 nm** and **2-visible**, respectively). The loss of activity at higher irradiation wavelengths is also due to the loss of UV absorption of complex **2** in this area.

In conclusion, complex **1** is the most active compound, and further studies regarding the potential mechanism of cleavage were carried out. It is supported that metal complexes cause efficient cleavage contrastingly to ligand (hydrazone compound) suggesting that metal binding is important for DNA degradation [71].

3.5.3 Mechanistic pDNA photo-cleavage studies

According to the pDNA photo-cleavage, complex **1** after irradiation with visible light induced the most pronounced cleavage effect. Therefore, further studies concerning the pDNA-cleavage ability of complex **1** after irradiation with visible light were performed in the co-existence of diverse factors that may possibly elucidate the cleavage mechanism; under argon atmosphere (i.e. anaerobic conditions) or in the presence of NaN_3 (singlet oxygen scavenger), or DMSO (hydroxyl radical scavenger).

The results (Fig. 9) have shown that the effect of complex **1** on DNA was restricted under anaerobic conditions (Fig. 9 lane 3). Under aerobic conditions, the mode of action most probably involves singlet oxygen rather than hydroxyl radicals (reaction with NaN_3 and DMSO, lanes 4 and 6 in Fig. 9, respectively). However, when D_2O was used as a solvent (Fig. 9, lane 5), the cleavage of DNA has not been enhanced, indicating that the mechanism of action may partially be *via* the formation of singlet oxygen, nevertheless a more complex mechanism of action is taking place.

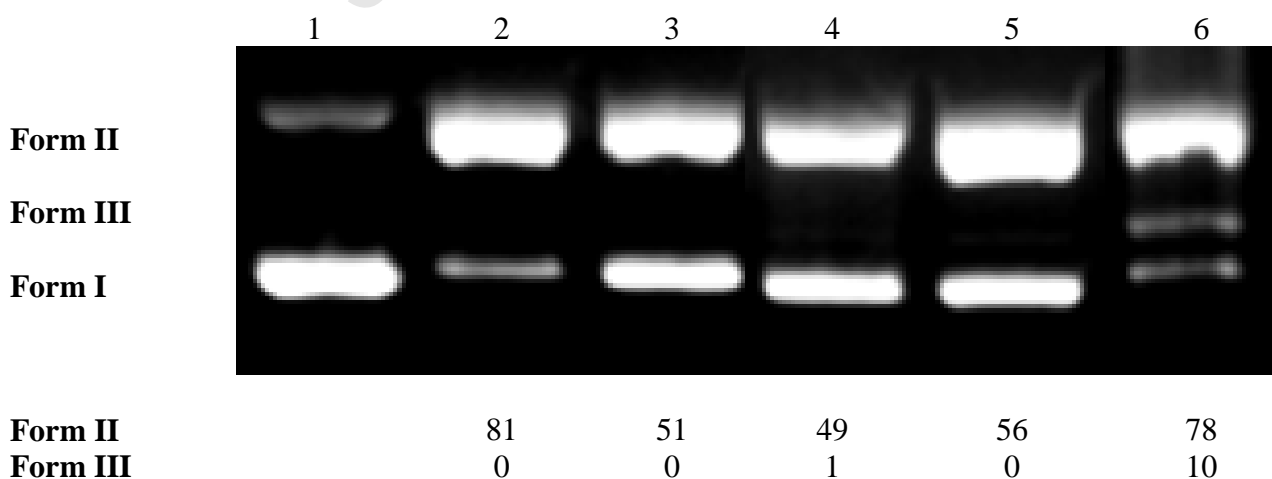


Fig. 9. Mechanistic studies regarding the DNA (pBLuescript KS II DNA) photo-cleavage induced by complex **1** (500 μ M) after irradiation with visible light. Gel electrophoresis pictures: Lane 1: pDNA; Lane 2: DNA + **1**; Lane 3: DNA + **1** + argon; Lane 4: DNA + **1** + NaN₃; Lane 5: DNA + **1** + D₂O; Lane 6: DNA + **1** + DMSO. Bottom: Calculation of the % conversion to ss and ds damage. DNA forms: Form I = supercoiled, Form II = relaxed, Form III = linear plasmid DNA.

3.6 Free radical scavenging

The presence of free radicals in the body is probably the principal reason initially for the development of inflammations and their side-effects [72]. The presence of compounds that can neutralize or scavenge free radicals is significant because they may protect cells from the attack of free radicals and may subsequently offer protection from the effects caused by radicals, such as ageing or chronic diseases including heart diseases and cancer [72]. Compounds that can act as free radicals scavengers or inhibitors of their production may serve for the treatment of inflammations. Taken into consideration that the quinazoline derivatives have exhibited anti-inflammatory activity [73,74], we have investigated the *in vitro* ability of **L** and its zinc complexes **1** and **2** to scavenge DPPH and ABTS radicals (Table 5). Furthermore, the radical scavenging activity of the compounds was compared with that of NDGA, BHT and trolox which are the most commonly used antioxidant agents as reference compounds.

Table 5. % DPPH-scavenging ability (DPPH%) and % ABTS radical scavenging activity (ABTS%) for **L** and its complexes **1** and **2**. All measurements were carried out in triplicate.

Compound	DPPH%, 30 min	DPPH%, 60 min	ABTS%
L	20.63±0.33	21.97±0.69	58.91±0.85
Complex 1	25.96±0.69	30.93±0.45	85.65±1.18
Complex 2	39.33±0.36	47.45±0.28	98.25±0.14
NDGA	87.08±0.12	87.47±0.12	Not tested
BHT	61.30±1.16	76.78±1.12	Not tested
Trolox	Not tested	Not tested	98.10±0.48

The DPPH-scavenging ability is correlated with the potential antiageing, anticancer and anti-inflammatory activity of the compounds [72]. The DPPH-scavenging ability of **L** was found time-independent, while for the complexes the DPPH-scavenging activity increased upon time. In addition, the complexes were much more active than free **L**. The compounds present low-to-moderate ability to scavenge DPPH radicals, when compared to the reference compounds NDGA and BHT. Complex [Zn(L)(dicl)₂] **2** shows the highest DPPH-scavenging activity among the complexes and may be considered a moderate DPPH-scavenger. The increased activity of complex **2** may obviously be ascribed to the presence of the diclofenac ligands.

The ABTS-scavenging activity is in many cases a marker of the total antioxidant activity [72]. The complexes are much more active ABTS-scavengers than free **L**. Complex **2** is the best ABTS-scavenger among the compounds under study presenting extremely high ABTS-scavenging ability similar to the reference compound trolox, the highest among the metal-NSAID complexes found in the literature [75]. The presence of the diclofenac co-ligands seems to be the main reason for the pronounced activity of complex **2** in comparison to complex **1**.

In conclusion, the Zn complexes **1** and **2** are more potent radical scavengers than the free **L**, indicating that enhanced scavenging activity towards DPPH and ABTS radicals may result from the coordination of **L** to Zn. In addition, among the complexes, complex **2** bearing the NSAID diclofenac is the most active radical scavenger and this may be attributed to the NSAID co-ligand leading to a higher synergism. Furthermore, the complexes seem to show selective scavenging activity of ABTS towards DDPH. Such conclusions are in good agreement with reports regarding the enhanced radical scavenging of metal complexes of bioactive ligands in comparison to the corresponding free ligands [30,42-44,75-78].

3.7 Albumin-binding properties of the compounds

3.7.1 Interaction of the compounds with BSA

The serum albumins (SAs) are of the most significant and abundant plasma proteins in blood stream having a plethora of functions including the maintenance of blood pH and colloidal osmotic pressure functions [79]. The albumin serves as carrier conjugate of various compounds such as hormones, fatty acids, ions and drugs that are poorly dissolved in water [79,80]; therefore, albumins may have wide clinical, pharmaceutical, and biochemical applications [81]. BSA is the most studied serum albumin in regard to the binding with bioactive compounds and is chosen because it is a human serum albumin homologue [82]. The solution of BSA exhibits an intense emission band located at $\lambda_{em,max} = 343$ nm when excited at 295 nm, due to the presence of tryptophan residues, the Trp-134 and Trp-212 in the first sub-domain IB and sub-domain IIA, respectively, for BSA [82,83].

The result of the addition of the compounds in the BSA-solution was a significant quenching of the BSA fluorescence emission band up to 85.6% of the initial fluorescence (representative spectra are shown in Fig. 10(A)). Furthermore, the inner-filter effect was evaluated with eq. S4 [61]; it was found negligible to affect the measurements.

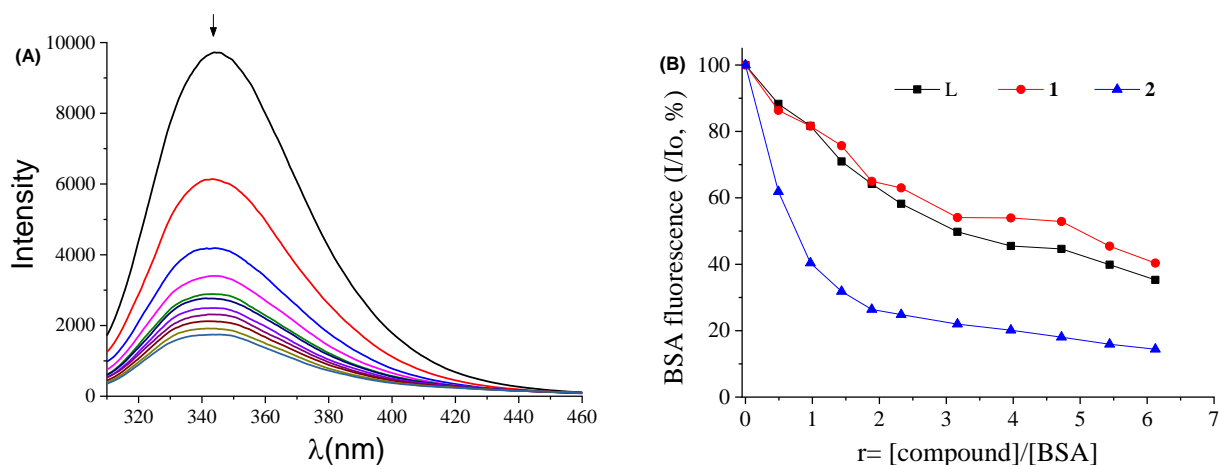


Fig. 10. (A) Fluorescence emission spectra ($\lambda_{\text{excitation}} = 295$ nm) for BSA ($[\text{BSA}] = 3 \mu\text{M}$) in buffer solution (150 mM NaCl and 15 mM trisodium citrate at pH 7.0) in the absence and presence of increasing amounts of complex **2**. The arrows show the changes of intensity upon increasing amounts of complex **2**. (B) Plot of % relative fluorescence intensity at $\lambda_{\text{em}} = 343$ nm (I/I_0 , %) versus r ($r = [\text{complex}]/[\text{BSA}]$) for **L** and its complexes **1** and **2** (up to 64.7% of the initial BSA fluorescence for **L**, 59.7% for **1** and 85.6% for **2**) in buffer solution (150 mM NaCl and 15 mM trisodium citrate at pH 7.0).

The observed quenching of the BSA emission band resulted from the addition of the compounds was moderate in the case of **L** and complex **1** and much more enhanced in the case complex **2** (of the initial BSA fluorescence emission ($\Delta I/I_0$) was up to 85.6 % (Fig. 10(B)). Such high quenching is usually attributed to possible changes around SA-tryptophan residues resulting from changes in albumin secondary structure due to the binding of the compounds to SA [84].

The quenching constants (k_q) concerning the interaction of the compounds with BSA were determined (Table 6) with the Stern-Volmer quenching equation (eqs. S2 and S3, taking as fluorescence lifetime of tryptophan in BSA $\tau_0 = 10^{-8}$ s [62]), and from the corresponding Stern-Volmer plots (Fig. S9). The obtained k_q constants are of the order $10^{13} \text{ M}^{-1}\text{s}^{-1}$ and are significantly higher than $10^{10} \text{ M}^{-1}\text{s}^{-1}$ indicating the existence of a static quenching mechanism [57] and subsequently verifying the interaction of the compounds complexes with BSA. The k_q constants may suggest that the compounds have significant BSA-quenching ability; with complex **2** presenting the highest k_q constant for BSA.

Table 6. The BSA-quenching (k_q) and BSA-binding (K) constants for **L** and complexes **1** and **2**.

Compound	k_q ($\text{M}^{-1}\text{s}^{-1}$)	K (M^{-1})
L	$1.05(\pm 0.03) \times 10^{13}$	$8.68(\pm 0.60) \times 10^4$
1	$0.76(\pm 0.04) \times 10^{13}$	$1.33(\pm 0.10) \times 10^5$
2	$3.04(\pm 0.14) \times 10^{13}$	$6.77(\pm 0.30) \times 10^5$

The values of the BSA-binding constants (K) of the compounds were calculated with Scatchard equation (eq. S5) and plots (Fig. S10). The BSA-binding constants of the compounds are relatively high (of the order 10^4 - 10^5 M^{-1}) with the complexes being better binders to BSA than HL. Furthermore, the magnitude of the K values of the compounds (8.68×10^4 - 6.77×10^5 M^{-1}) may indicate their tight and reversible binding to albumins, when compared with the limit value of $K \approx 10^{15}$ M^{-1} for the strongest known non-covalent interactions, i.e. among avidin and diverse ligands, so that they can get released upon arrival at the desired biotargets [85].

3.7.2 Location of the BSA-binding site

Albumins have been crystallographically defined in three domains (I, II and III) and each domain is subdivided in two subdomains (A and B) [86]. There are at least four sites in the albumin where drugs and metal ions can be bound. The most important sites where drugs are bound are Sudlow's site 1 (or drug site I) located in subdomain IIA and Sudlow's site 2 (or drug site II) located in subdomain IIIA [86]. Warfarin and ibuprofen are the most prevalent markers of the BSA-binding site since they show high binding affinity for sites I and II, respectively [87].

The BSA subdomain where **L** and complexes **1** and **2** may bind to BSA can be specified by competitive experiments with warfarin and ibuprofen by fluorescence emission spectroscopy. The addition of **L** and complexes **1** and **2** to a pre-treated solution containing BSA and the site-probe resulted in a significant quenching of the initial fluorescence emission band (representatively shown for complex **2** in Fig. 11).

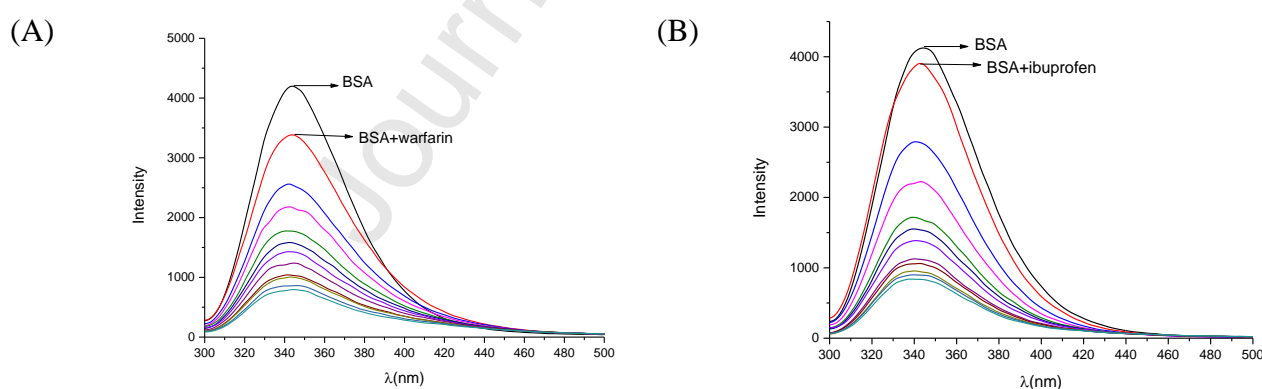


Fig. 11. (A) Fluorescence emission spectra ($\lambda_{\text{excitation}} = 295$ nm) for BSA ($3 \mu\text{M}$) in the presence of warfarin ($3 \mu\text{M}$) in buffer solution (150 mM NaCl and 15 mM trisodium citrate at pH 7.0) upon addition of increasing amounts of complex **2**. The arrow shows the changes of intensity upon increasing amounts of complex. (B) Fluorescence emission spectra ($\lambda_{\text{excitation}} = 295$ nm) for BSA ($3 \mu\text{M}$) in the presence of ibuprofen ($3 \mu\text{M}$) in buffer solution (150 mM NaCl and 15 mM trisodium citrate at pH 7.0) upon addition of increasing amounts of complex **2**. The arrows show the changes of intensity upon increasing amounts of complex.

The BSA-binding constants of the compounds in the presence of warfarin or ibuprofen were calculated with the Scatchard equation (eq. S5) and plots (Figs. S11 and S12) and their values are given in Table 7 and are compared with those determined in the absence of any site-marker. A decrease of the value of K in presence of the site-marker shows that the binding of the compound to albumin is influenced by the presence of this marker due to competition for the same binding site [78,87].

Table 7. BSA-binding constants of the compounds (K , in M^{-1}) in the absence or presence of the site probes warfarin and ibuprofen.

Compound	No probe - K (M^{-1})	Probe: warfarin - K (M^{-1})	Probe: ibuprofen - K (M^{-1})
L	$8.68(\pm 0.60) \times 10^4$	$1.03(\pm 0.07) \times 10^5$	$5.18(\pm 0.30) \times 10^4$
1	$1.33(\pm 0.10) \times 10^5$	$1.32(\pm 0.08) \times 10^5$	$2.72(\pm 0.19) \times 10^4$
2	$6.77(\pm 0.30) \times 10^5$	$2.44(\pm 0.06) \times 10^5$	$2.93(\pm 0.11) \times 10^5$

More specifically, the BSA-binding constants of **L** and complex **1** decreased significantly in the presence of ibuprofen, suggesting that the most possible binding site of these compounds to BSA is Sudlow's site 2 in subdomain IIIA. In the case of complex **2**, the binding constants decrease in both cases, suggesting that the complex can be bound in both sites without showing any selectivity [78,87].

4 Conclusions

A novel *o*-pyridine-hydrazone derivative of 4-quinazoline ligand has been synthesized and its interaction with Zn^{2+} resulted in the formation of the dicationic $[Zn(L)_2](NO_3)_2 \cdot MeOH$ (**1**·MeOH), where the quinazoline **L** was tridentately bound to Zn(II) through the quinazoline, the hydrazone and the pyridine nitrogen atoms. When NSAID Nadicl was involved in this reaction, the neutral complex $[Zn(L)(dicl-O)_2] \cdot MeOH$ (**2**·MeOH) was isolated, where diclofenac is monodentately bound to Zn(II) *via* a carboxylate oxygen and **L** was bound in a manner similar to complex **1**.

The interaction of the **L** and its complexes **1** and **2** with CT DNA was performed by UV-vis spectroscopy, viscosity measurements and EB-displacement studies. It has been concluded that the complexes may be bound with CT DNA *via* intercalation. Complex **1** has higher DNA-binding constant than complex **2** showing that it is a better DNA-binder than **2**.

The interaction of the compounds with supercoiled circular pBluescript KS II plasmid DNA was studied by agarose gel electrophoresis experiments in the absence or presence of irradiation with UVB (312 nm), UVA (365 nm) or visible light. Both complexes exhibited better pDNA photocleavage activity compared to quinazoline **L** which in most cases was practically inactive.

Especially complex **1** was the most active compound for both studied concentrations and for all different conditions (presence/absence and λ of irradiation), due to a mechanism of photo-action that implicates also singlet oxygen.

The ability of the compounds to scavenge the DPPH and ABTS free radicals was studied; complex **2** bearing the NSAID diclofenac was the best scavenger among the compounds tested.

The ability of the compounds to bind to BSA was explored and the BSA-binding site of the compounds was investigated *via* competitive studies with the typical site-probes warfarin and ibuprofen. The compounds can bind tightly and reversibly to BSA in order to get transferred towards potential biological targets. The quinazoline derivative **L** and complex **1** prefer to bind to BSA at Sudlow's site 2 in subdomain IIIA in competition to ibuprofen, while complex **2** can bind either at Sudlow's site 2 in subdomain IIIA or at Sudlow's site 1 in subdomain IIA in competition to ibuprofen or warfarin, respectively.

From the existing data, it seems that the hybride molecule quinazoline-hydrazone-*o*-pyridine (**L**) fulfills primarily the structural requirements for efficient complexation with Zn either with itself or with other ligands in a synergistic way. Depending on the choice of the second ligand (**L** or Nadicl) the biological activities seem to alter, allowing the designing of possible DNA binders, cleavers and photo-cleavers or radical scavengers.

It is important to note that hybride molecule **L** may play the role of a lead ligand compound eligible to improvement *via* derivatization in both quinazoline and *o*-pyridine. This, in combination with other metals and NAIDs may allow the discovery of novel anti-cancer or PDT agents and/or NAIDs with improved activities.

Acknowledgement

The author CK acknowledges the financial support *via* a scholarship from the General Secretariat for Research and Technology (GSRT) and Hellenic Foundation for Research and Innovation (HFRI), Greek Ministry of Education, Research and Religion.

Conflict of Interest

There are no conflicts to declare.

Abbreviations

ABTS	2,2'-azinobis-(3-ethylbenzothiazoline-6-sulfonic acid)
BHT	butylated hydroxytoluene
BSA	bovine serum albumin
CT	calf-thymus

dicl ⁻	anion of diclofenac
DPPH	1,1-diphenyl-picrylhydrazyl
ds	double-stranded
EB	ethidium bromide
HRMS	High-resolution mass spectra
K	BSA-binding constant
K _b	DNA-binding constant
k _q	quenching constant
K _{SV}	Stern-Volmer constant
L	(<i>E</i>)-4-(2-(pyridin-2-ylmethylene)hydrazinyl)quinazoline
Nadicl	sodium diclofenac
NDGA	nordihydroguaiaretic acid
NSAID	non-steroidal anti-inflammatory drug
pDNA	pBluescript KS II plasmid DNA
<i>r</i>	[complex]/[DNA] ratio or [complex]/[BSA]
<i>r</i> '	[DNA]/[compound]
SA	serum albumin
sh	shoulder
ss	single-stranded
trolox	6-hydroxy-2,5,7,8-tetramethylchromane-2-carboxylic acid
$\Delta v(\text{CO}_2)$	$v_{\text{asym}}(\text{CO}_2) - v_{\text{sym}}(\text{CO}_2)$
λ_{ex}	excitation wavelength
τ_0	fluorescence lifetime

Appendix A. Supplementary material

CCDC 2002629 and 2002630 contain the supplementary crystallographic data for compounds **1** and **2**, respectively. These data can be obtained free of charge *via* www.ccdc.cam.ac.uk/conts/retrieving.html (or from the Cambridge Crystallographic Data Centre, 12 Union Road, Cambridge CB21EZ, UK; fax: (+44) 1223-336-033; or deposit@ccdc.cam.ac.uk). Supplementary data associated with this article can be found, in the online version, at doi:

References

- [1] S. Ravez, O. Castillo-Aguilera, P. Depreux, L. Goossens, Expert Opinion on Therapeutic Patents 25 (2015) 789-804.
- [2] P. Griess, Berichte 2 (1869) 415-418.

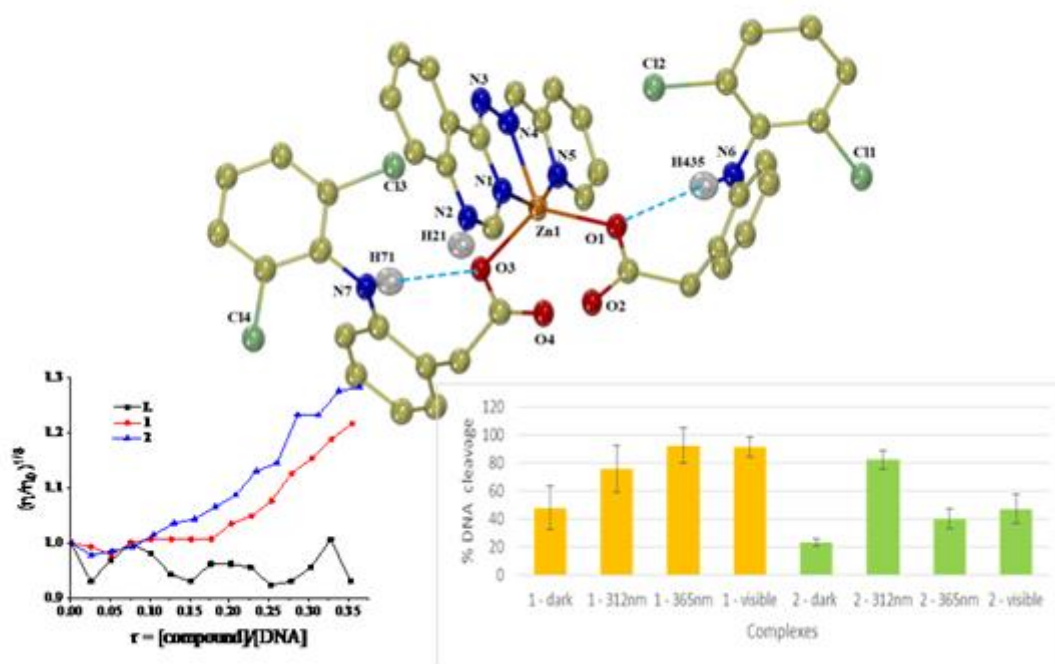
- [3] S. Gabriel, J. Colman, *Chem. Ber.* 36 (1903) 3379-3385.
- [4] D. Wang, F. Gao, *Chem. Cent. J.* 7 (2013) 95-110.
- [5] X. Su, I. Aprahamian, *Chem. Soc. Rev.* 43 (2014) 1963-1981.
- [6] R.M. Shivshankar, *J. Crit. Rev.* 6 (2019) 1-4.
- [7] S.J. Sonawane, R.S. Kalhapure, T. Govender, *Eur J Pharm Sci.* 199 (2017) 45-65.
- [8] M.A.W. Lawrence, S.C. Lorraine, K. Wilson, K. Wilson, *Polyhedron*, 2019, 173, 114111
- [9] M.E.M. Shakdofa. M.H. Shtaiwi. N. Morsy, M.A.T. Abdel-rassel, *Main Group Chem.* 13 (2014) 187-218.
- [10] S. Rollas, S.G. Kucukguzel, *Molecules* 12 (2007) 1910-1939.
- [11] L. Popiolek, *Med. Chem. Res.* 26 (2017) 287-301.
- [12] G. Verma, A. Marella, M. Shaquiquzzaman, M. Akhtar, M.R. Ali, M.M. Alam, *J. Pharm. Bioall. Sci.* 6 (2014) 69-80.
- [13] M. Fares, W.M. Eldehna, S.M. Abou- Seri, H.A. Abdel- Aziz, M.H. Aly, M.F. Tolba, *Arch. Pharm (Weinheim)* 348 (2015) 144-154.
- [14] A.E. Kümmerle, M. Schmitt, S.V.S. Cardozo, C. Lugnier, P. Villa, A.B. Lopes, N.C. Romeiro, H. Justiniano, M.A. Martins, C.A.M. Fraga, J. Bourguignon, E.J. Barreiro, *J. Med. Chem.* 55 (2012) 7525-7545.
- [15] J. Kimura, H. Yamada, H. Ogura, T. Yajima, T. Fukushima, *Anal. Chim. Acta* 635 (2009) 207-213.
- [16] H. Yamada, A. Shirai, K. Kato, J. Kimura, H. Ichiba, T. Yajima, T. Fukushima, *Chem. Pharm. Bull.* 58 (2010) 875-878.
- [17] T.V. Trashakhova, E.V. Nosova, P.A. Slepukhin, M.S. Valova, G.N. Lipunova, V.N. Charushin, *Russ. Chem. Bull., Int. Ed.* 60 (2011) 2347-2353.
- [18] Y. Cherasse, Y. Urade, *Int. J. Mol. Sci.* (2017) 18 2334.
- [19] I. Bertini, A. Sigel, H. Sigel (Eds.), *Handbook on Metalloproteins*, Marcel Dekker, Inc., New York and Basel, (2001) Chapter 19, pp. 881–959.
- [20] E. Freisinger, R.K.O. Sigel, *Chimia* 73 (2019) 1-9.
- [21] N.N. Greenwood, A. Earnshaw, *Chemistry of the Elements* (2nded.), Oxford, Butterworth-Heinemann, (1997).
- [22] K.M. Hambidge, N.F. Krebs, *J. Nutr.* 137 (2007) 1101-1105.
- [23] B. Rosenberg, *Interdiscip. Sci. Rev.* 3 (1978) 134–147.
- [24] X. Wang, X. Wang, Z. Guo, *Acc. Chem. Res.* 48 (2015) 2622-2631.
- [25] H. Liu, Y. Qu, X. Wang, *Future Med. Chem.* 10 (2018) 679-701.
- [26] C.P. Larson, U.R. Saha, H. Nazrul, *PLoS Medicine* 6 (2009) e1000175.

- [27] H. Sakurai, Y. Kojima, Y. Yoshikawa, K. Kawabe, H. Yasui, *Coord. Chem. Rev.* 226 (2002) 187-198.
- [28] Q. Zhou, T.W. Hambley, B.J. Kennedy, P.A. Lay, P. Turner, B. Warwick, J.R. Biffin, H.L. Regtop, *Inorg. Chem.* 39 (2000) 3742-3748.
- [29] A. Tarushi, K. Lafazanis, J. Klun, I. Turel, A.A. Pantazaki, G. Psomas, D.P. Kessissoglou, J. *Inorg. Biochem.* 121 (2013) 53-65.
- [30] A. Tarushi, C. Kakoulidou, C.P. Raptopoulou, V. Psycharis, D.P. Kessissoglou, I. Zoi, A.N. Papadopoulos, G. Psomas, *J. Inorg. Biochem.* 170 (2017) 85-97.
- [31] J.S. Casas, E.E. Castellano, M.D. Couce, J. Ellena, A. Sanchez, J. Sordo, C. Taboada, J. *Inorg. Biochem.* 100 (2006) 124-132.
- [32] K. Gurova, *Future Oncology* 5 (2009) 1685-1704.
- [33] J.G. Hardman, L.E. Limbird (eds), Goodman and Gilman's the Pharmacological Basis of Therapeutics (10thed), McGraw Hill (2001).
- [34] B.M. Zeglis, V.C. Pierre, J.K. Barton, *Chem. Commun.* (2007) 4565-4579.
- [35] D.R. Boer, A. Canals, M. Coll, *Dalton Trans.* (2009) 399-414.
- [36] S.S. Lucky, K.C. Soo, Y. Zhang, *Chem. Rev.* 115 (2015) 1990-2042.
- [37] C. Wende, C. Ludtke, N. Kulak, *Eur. J. Inorg. Chem.* (2014) 2597-2612
- [38] G. Chen, Z. Wang, Y. Kou, J. Tian, S. Yan, *J. Inorg. Biochem.* 122 (2013) 49-56.
- [39] W.J. Wechter, E.D. Murray, D. Kantoci, D.D. Quiggle, D.D. Leipold, K.M. Gibson, J.D. McCracken, *Life Sci.* 66 (2000) 745-753.
- [40] E. Echenique-Errandonea, I. Oyarzabal, J. Cepeda, E.S. Sebastian, A.R. Dieguez, J.M. Seco, *New J. Chem.* 41 (2017) 5467-5475.
- [41] S. Sayen, A. Carlier, M. Tarpin, E. Guillon, *J. Inorg. Biochem.* 120 (2013) 39-43.
- [42] F. Dimiza, F. Perdih, V. Tangoulis, I. Turel, D.P. Kessissoglou, G. Psomas, *J. Inorg. Biochem.* 105 (2011) 476-489.
- [43] S. Kumar, R.P. Sharma, P. Venugopalan, V. Ferretti, S. Perontsis, G. Psomas, *J. Inorg. Biochem.* 187 (2018) 97-108.
- [44] M. Zampakou, A.G. Hatzidimitriou, A.N. Papadopoulos, G. Psomas, *J. Coord. Chem.* 68 (2015) 4355-4372.
- [45] A. Tarushi, A.G. Hatzidimitriou, M. Estrader, D.P. Kessissoglou, V. Tangoulis, G. Psomas, *Inorg. Chem.* 56 (2017) 7048-7057.
- [46] D. Kovala-Demertzi, D. Mentzafos, A. Terzis, *Polyhedron* 12 (1993) 1361-1370.
- [47] N. Kourkoumelis, M.A. Demertzis, D. Kovala-Demertzi, A. Koutsodimou, A. Moukarika, *Spectrochim. Acta A* 60 (2004) 2253-2259.

- [48] M. Kyropoulou, C.P. Raptopoulou, V. Psycharis, G. Psomas, *Polyhedron* 61 (2013) 126-136.
- [49] J. Marmur, *J. Mol. Biol.* 3 (1961) 208-211.
- [50] M.F. Reichmann, S.A. Rice, C.A. Thomas, P. Doty, *J. Am. Chem. Soc.* 76 (1954) 3047-3053.
- [51] Y. Loidreau, T. Besson, *Tetrahedron* 67 (2011) 4852-4857.
- [52] J. He, X. Wang, X. Zhao, Y. Liang, H. He, L. Fu, *Eur. J. Med. Chem.* 54 (2012) 925-930.
- [53] Bruker Analytical X-ray Systems, Inc. Apex2, Version 2 User Manual, M86-E01078, Madison, WI, (2006).
- [54] L. Palatinus, G. Chapuis, *J. Appl. Cryst.* 40 (2007) 786-790.
- [55] P.W. Betteridge, J.R. Carruthers, R.I. Cooper, K. Prout, D.J. Watkin, *J. Appl. Cryst.* 36 (2003) 1487.
- [56] A. Wolfe, G. Shimer, T. Meehan, *Biochemistry* 26 (1987) 6392-6396.
- [57] J.R. Lakowicz, *Principles of Fluorescence Spectroscopy*, third ed., Plenum Press, New York (2006).
- [58] D.P. Heller, C.L. Greenstock, *Biophys. Chem.* 50 (1994) 305-312.
- [59] A. Papastergiou, S. Perontsis, P. Gritzapis, A. E. Koumbis, M. Koffa, G. Psomas, K. C. Fylaktakidou, *Photochem. Photobiol. Sci.* 15 (2016) 351-360.
- [60] C. Kontogiorgis, D. Hadjipavlou-Litina, *J. Enz. Inhib. Med. Chem.* 18 (2003) 63-69.
- [61] L. Stella, A.L. Capodilupo, M. Bietti, *Chem. Commun.* (2008) 4744-4746.
- [62] Y. Wang, H. Zhang, G. Zhang, W. Tao, S. Tang, *J. Luminescence* 126 (2007) 211-218.
- [63] S.D. Barchechath, R.I. Tawatao, M. Corr, D.A. Carson, H.B. Cottam, *J. Med. Chem.* 48 (2005) 6409-6422.
- [64] W.J. Geary, *Coord. Chem. Rev.* 7 (1971) 81-122.
- [65] K. Nakamoto, *Infrared and Raman Spectra of Inorganic and Coordination Compounds, Part B: Applications in Coordination, Organometallic, and Bioinorganic Chemistry*, 6th ed., Wiley, New Jersey (2009).
- [66] A. Szorcsik, L. Nagy, J. Sletten, G. Szalontai, E. Kamu, T. Fiore, L. Pellerito, E. Kalman, *J. Organomet. Chem.* 689 (2004) 1145-1154.
- [67] A.W. Addison, T.N. Rao, J. Reedijk, J. van Rijn, G.C. Verchoor, *J. Chem. Soc., Dalton Trans.* (1984) 1349-1356.
- [68] A.M. Pyle, J.P. Rehmann, R. Meshoyrer, C.V. Kumar, N.J. Turro, J.K. Barton, *J. Am. Chem. Soc.* 111 (1989) 3053-3063.
- [69] A. Dimitrakopoulou, C. Dendrinou-Samara, A.A. Pantazaki, M. Alexiou, E. Nordlander, D.P. Kessissoglou, *J. Inorg. Biochem.* 102 (2008) 618-628.

- [70] P. Zivec, F. Perdih, I. Turel, G. Giester, G. Psomas, *J. Inorg. Biochem.* 117 (2012) 35-47.
- [71] V. Sumalatha, A. Rambabu, N. Vamsikrishna, N. Ganji, S. Daravath, Shivaraj, *Chemical Data Collections* 20 (2019) 100213.
- [72] R. Cini, G. Giorgi, A. Cinquantini, C. Rossi, M. Sabat, *Inorg. Chem.* 29 (1990) 5197-5200.
- [73] A.M. Alafeefy, A.A. Kadi, O.A. Al-Deeb, K.E.H. El-Tahir, N.A. Al-jaber, *Eur. J. Med. Chem.* 45 (2010) 4947-4952.
- [74] M.M. Gineinah, M.A. El-Sherbeny, M.N. Nasr, A.R. Maarouf, *Arch. Pharm. Pharm. Med. Chem.* 11 (2002) 556-562.
- [75] G. Psomas, *Coord. Chem. Rev.* 412 (2020) 213259.
- [76] M. Lazou, A.G. Hatzidimitriou, A.N. Papadopoulos, G. Psomas, *J. Inorg. Biochem.* 195 (2019) 101-110.
- [77] F. Dimiza, M. Lazou, A.N. Papadopoulos, A.G. Hatzidimitriou, G. Psomas, *J. Inorg. Biochem.* 203 (2020) ID 110905.
- [78] M. Lazou, A. Tarushi, P. Gritzapis, G. Psomas, *J. Inorg. Biochem.* 206 (2020) 111019.
- [79] X. He, D.C. Carter, *Nature* 358 (1992) 209-215.
- [80] R.E. Olson, D.D. Christ, *Ann. Rep. Med. Chem.* 31 (1996) 327-336.
- [81] K.A. Majorek, P.J. Porebski, A. Dayal, M.D. Zimmerman, K. Jablonska, A.J. Stewart, M. Chruszcz, W. Minor, *Mol. Immunol.* 52 (2012) 174-182.
- [82] C. Tan, J. Liu, H. Li, W. Zheng, S. Shi, L. Chen, L. Ji, *J. Inorg. Biochem.* 102 (2008) 347-358.
- [83] I. Petitpas, T. Grune, A.A. Bhattacharya, S. Twine, M. East, S. Curry, *J. Mol. Biol.* 314 (2001) 955-960.
- [84] V. Rajendiran, R. Karthik, M. Palaniandavar, H. Stoeckli-Evans, V.S. Periasamy, M.A. Akbarsha, B.S. Srinag, H. Krishnamurthy, *Inorg. Chem.* 46 (2007) 8208-8221.
- [85] O.H. Laitinen, V.P. Hytönen, H.R. Nordlund, M.S. Kulomaa, *Cell. Mol. Life Sci.* 63 (2006) 2992-3017.
- [86] G. Sudlow, D.J. Birkett, D.N. Wade, *Mol. Pharmacol.* 12 (1976) 1052-1061.
- [87] N. Shahabadi, B. Bazvandi, A. Taherpour, *J. Coord. Chem.* 70 (2017) 3186-3198.

Graphical abstract



A novel *o*-pyridine-hydrazone derivative of 4-quinazoline and its Zn(II) complexes in the absence or presence of diclofenac were characterized and were evaluated for their affinity to bovine serum albumin, calf-thymus DNA and plasmid-DNA in the absence or presence of irradiation as well as their ability to scavenge free radicals.

Research highlights

- A novel **quinazoline and its two Zn complexes were prepared and characterized.**
- Intercalation is the most possible binding mode of the complexes to DNA
- The complexes exhibit noteworthy plasmid DNA photocleavage activity
- The compounds may bind tightly and reversibly to bovine serum albumin.
- The antioxidant activity of complexes depends on the presence of diclofenac ligand.

Journal Pre-proof